Accepted Manuscript

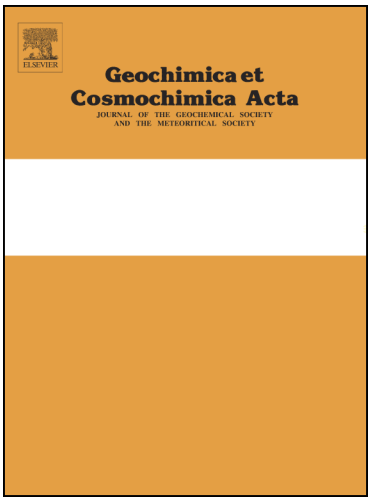

Temporal record of osmium concentrations and $^{187}Os/^{188}Os$ in organic-rich mudrocks: Implications for the osmium geochemical cycle and the use of osmium as a paleoceanographic tracer

Xinze Lu, Brian Kendall, Holly J. Stein, Judith L. Hannah

PII: S0016-7037(17)30405-2
DOI: http://dx.doi.org/10.1016/j.gca.2017.06.046
Reference: GCA 10359

To appear in: *Geochimica et Cosmochimica Acta*

Received Date: 19 December 2016
Revised Date: 24 June 2017
Accepted Date: 27 June 2017

Please cite this article as: Lu, X., Kendall, B., Stein, H.J., Hannah, J.L., Temporal record of osmium concentrations and $^{187}Os/^{188}Os$ in organic-rich mudrocks: Implications for the osmium geochemical cycle and the use of osmium as a paleoceanographic tracer, *Geochimica et Cosmochimica Acta* (2017), doi: http://dx.doi.org/10.1016/j.gca.2017.06.046

Temporal record of osmium concentrations and $^{187}Os/^{188}Os$ in organic-rich mudrocks: Implications for the osmium geochemical cycle and the use of osmium as a paleoceanographic tracer

Xinze Lu[1]*, Brian Kendall[1], Holly J. Stein[2,3], Judith L. Hannah[2,3]

[1] *Department of Earth and Environmental Sciences, 200 University Avenue West, University of Waterloo, Waterloo, ON N2L 3G1, Canada*

[2] *AIRIE Program, Colorado State University, Fort Collins, CO 80523-1482, USA*

[3] *Centre for Earth Evolution and Dynamics, University of Oslo, 0316 Oslo, Norway*

Re-submitted to *Geochimica et Cosmochimica Acta*

Special Issue: HSE Earth and Planets

June 24, 2017

* Corresponding Author at: Department of Earth and Environmental Sciences, University of Waterloo, 200 University Avenue West, Waterloo, Ontario, Canada N2L 3G1. Email address: xlv@uwaterloo.ca

Abstract

We present a compilation of ^{192}Os concentrations (representing non-radiogenic Os) and initial $^{187}Os/^{188}Os$ isotope ratios from organic-rich mudrocks (ORM) to explore the evolution of the Os geochemical cycle during the past three billion years. The initial $^{187}Os/^{188}Os$ isotope ratio of a Re-Os isochron regression for ORM constrains the local paleo-seawater $^{187}Os/^{188}Os$, which is governed by the relative magnitudes of radiogenic Os (old continental crust) and unradiogenic Os (mantle, extraterrestrial, and juvenile/mafic/ultramafic crust) fluxes to seawater. A first-order increase in seawater $^{187}Os/^{188}Os$ ratios occurs from the Archean to the Phanerozoic, and may reflect a combination of increasing atmosphere-ocean oxygenation and weathering of progressively more radiogenic continental crust due to in-growth of ^{187}Os from radioactive decay of ^{187}Re. Superimposed on this long-term trend are shorter-term fluctuations in seawater $^{187}Os/^{188}Os$ ratios as a result of climate change, emplacement of large igneous provinces, bolide impacts, tectonic events, changes in seafloor spreading rates, and lithological changes in crustal terranes proximal to sites of ORM deposition. Ediacaran-Phanerozoic ORM have mildly higher ^{192}Os concentrations overall compared with pre-Ediacaran Proterozoic ORM based on the mean and 95% confidence interval of 10,000 median values derived using a bootstrap analysis for each time bin (insufficient Archean data exist for robust statistical comparisons). However, there are two groups with anomalously high ^{192}Os concentrations that are distinguished by their initial $^{187}Os/^{188}Os$ isotope ratios. Ediacaran-Cambrian ORM from South China have radiogenic

initial $^{187}Os/^{188}Os$, suggesting their high ^{192}Os concentrations reflect proximal Os-rich crustal source(s), ultraslow sedimentation rates, and/or other unusual depositional conditions. In contrast, the unradiogenic initial $^{187}Os/^{188}Os$ and high ^{192}Os concentrations of some Mesozoic ORM can be tied to emplacement of large igneous provinces. Excluding these two anomalous groups and repeating the bootstrap analysis, we find that, overall, the ^{192}Os concentrations for the Ediacaran-Phanerozoic and pre-Ediacaran Proterozoic time bins are not significantly different. An improved understanding of Os geochemical behavior in modern environments is required before our compilation can be fully used to constrain the temporal evolution of the seawater Os reservoir.

1. INTRODUCTION

Variations in the seawater reservoir of trace metals through time reflect the interplay of multiple factors, including atmosphere-ocean O_2 levels, biological evolution, biogeochemical cycles, climate change (greenhouse/icehouse states), shifts in the relative fluxes of crustal versus mantle inputs to seawater during tectonic reorganizations and emplacement of large igneous provinces, and the growth and chemistry of the oceanic and continental crust (see the recent review by Robbins et al., 2016). First-order temporal changes in seawater trace metal reservoirs (i.e., on timescales of >> 100 Myr) can be inferred from first-order trends in the trace metal concentrations of marine sedimentary rocks such as organic-rich mudrocks (ORM) or iron formations if the depositional environment of these sedimentary rocks are reasonably well understood. Recently, such

temporal compilations have been presented for several trace metals that are bioessential and/or redox-sensitive (e.g., Mo, Ni, Zn, U, V, Cr, Co, Se; Scott et al., 2008; Konhauser et al., 2009, 2015; Sahoo et al., 2012; Partin et al., 2013a, 2013b; Reinhard et al., 2013; Robbins et al., 2013; Scott et al., 2013; Swanner et al., 2014; Large et al., 2014, 2015; Stüeken et al., 2015; Robbins et al., 2016; D. Tang et al., 2016).

The marine geochemical cycle of each trace metal has evolved in a unique fashion that reflects that metal's geochemical behavior and oceanic mass balance. For example, distinctive first-order increases in the Mo, Se, U, and V concentrations of ORM (bulk rock and/or pyrite data) occur at the beginning and end of the Proterozoic Eon. This observation suggests that the seawater concentrations of these metals increased following the Great Oxidation Event (GOE) because of increased riverine inputs from oxidative continental weathering, and following the Neoproterozoic Oxidation Event (NOE) because of possible further increases in riverine inputs, increased ocean oxygenation, and a smaller areal extent of anoxic seafloor where these metals are most efficiently removed to sediments (Scott et al., 2008; Sahoo et al., 2012; Partin et al., 2013a; Large et al., 2014; Stüeken et al., 2015).

By contrast, the seawater concentration of the bioessential trace metals Co and Ni may have decreased from the Archean to the Phanerozoic (Konhauser et al., 2009, 2015; Swanner et al., 2014; Large et al., 2014). During the Archean, there may have been a greater proportion of Ni- and Co-rich ultramafic rocks in seafloor hydrothermal systems, and the hydrothermal alteration of these rocks may have maintained sizable Ni and Co

seawater reservoirs (Konhauser et al., 2009, 2015; Kamber, 2010; Swanner et al., 2014). Subsequently, a switch to basalt-dominated hydrothermal systems due to cooler upper mantle temperatures may have decreased the flux of hydrothermal Co and Ni to the oceans. These interpretations are consistent with the observation that intervals of higher Co and Ni concentrations in sedimentary pyrite correlate with times of increased emplacement of large igneous provinces (Large et al., 2014).

Osmium is a transition metal in the platinum group of elements that exhibits redox-sensitive behavior but is not biologically important, which is not surprising given its extremely low concentration (pg/g levels) in the crust compared with most other trace metals (µg/g levels). Osmium is unique compared with other redox-sensitive trace metals in that it can be used as a radiogenic isotope tracer. Specifically, seawater $^{187}Os/^{188}Os$ can be used to constrain the relative fluxes to seawater of radiogenic Os from old felsic continental crust versus unradiogenic Os from the mantle, extraterrestrial material, and juvenile, mafic, and ultramafic crust (Peucker-Ehrenbrink and Ravizza, 2000). Many studies have discussed secular changes in seawater $^{187}Os/^{188}Os$ on billion-year timescales including the Precambrian (e.g., Kendall et al., 2009b; van Acken et al., 2013; Sperling et al., 2014; Stein and Hannah, 2014). Nevertheless, the temporal evolution of the marine Os geochemical cycle has not yet been explored from the perspective of Os enrichments in sedimentary archives because of insufficient data and a relatively poor understanding of the Os geochemical cycle compared with other redox-sensitive trace metals (e.g., Yang et al., 2009). Recent rapid growth in the number of Os studies, however, has helped

alleviate some of these shortcomings. In addition to Os concentration and isotope data, the ^{187}Re-^{187}Os geochronometer in ORM can yield depositional ages and confirm closed-system behavior since the time of deposition (e.g., Cohen et al., 1999; Anbar et al., 2007; Kendall et al., 2009a, 2009b; Stein and Hannah, 2014). Both advantages can be exploited simultaneously by Re-Os isochron regression of a suite of samples from a stratigraphically-restricted (typically < 1 m) and conformable (no stratigraphic discontinuities) interval of ORM, with the initial ^{187}Os/^{188}Os ratio from the regression providing the ^{187}Os/^{188}Os of contemporaneous local seawater (see Hannah and Stein, 2012 for a review).

In this study, we review current knowledge on the marine Os geochemical cycle, including the fluxes of individual Os sources and sinks, and estimates of the oceanic residence time of Os based on total input and output fluxes. We present compilations of both ^{192}Os concentrations (representing non-radiogenic Os at the time of deposition) and initial ^{187}Os/^{188}Os from ORM to evaluate temporal trends over the past three billion years. We explore the implications of our compilation for the evolution of the Os geochemical cycle and the use of Os as a paleoceanographic tracer.

2. MARINE GEOCHEMISTRY OF OSMIUM

2.1. Seawater Os concentrations and ^{187}Os/^{188}Os

In oxygenated seawater, Os accumulates as an octavalent oxyanion, an Os(IV) chloride complex, and/or an organocomplex, with an average concentration of ~10 pg/kg

(range of 6−14 pg/kg; Koide et al., 1991; Sharma et al., 1997; Levasseur et al., 1998, 1999; Woodhouse et al., 1999; Yamashita et al., 2007; Chen and Sharma, 2009; Sharma, 2012; Georg et al., 2013). The Os concentration of Pacific, Atlantic, and Southern seawater is not uniform with depth (maximum concentrations occur in the middle water column), suggesting non-conservative behavior for Os in the oceans (Chen and Sharma, 2009).

The $^{187}Os/^{188}Os$ of the modern deep ocean is ~ 1.05 (Sharma et al., 1997; Levasseur et al., 1999; Woodhouse et al., 1999; Peucker-Ehrenbrink and Ravizza, 2000; Chen et al., 2009). Seawater does not have a globally homogeneous $^{187}Os/^{188}Os$. Lower $^{187}Os/^{188}Os$ has been observed in surface ocean waters (~ 0.95) compared with deeper waters (~ 1.05), likely due to anthropogenic inputs to surface waters (Chen et al., 2009). Regional (non-anthropogenic) variations of modern and late Pleistocene open-ocean seawater $^{187}Os/^{188}Os$ have also been reported (Paquay and Ravizza, 2012; Rooney et al., 2016). In restricted basins and coastal regions, seawater $^{187}Os/^{188}Os$ can be locally different from deep open ocean seawater because of highly heterogenous local riverine Os inputs and/or groundwater discharge to seawater (Ravizza et al., 1991; Martin et al., 2000; Poirier, 2006; Paul et al., 2010; Rooney et al., 2016).

2.2. Sources of Os to Seawater

There are seven sources of Os to modern seawater: 1) oxidative weathering of the upper continental crust followed by riverine transport, 2) groundwater discharge, 3) high-

temperature and low-temperature submarine hydrothermal systems on the ocean floor, 4) aeolian dust, 5) cosmic dust, 6) volcanic aerosols, and 7) anthropogenic sources (Levasseur et al., 1999; Peucker-Ehrenbrink and Ravizza, 2000; Chen and Sharma, 2009; Paul et al., 2010; Rauch et al., 2010; Stein and Hannah, 2014). Precipitation is not included as it is not strictly an end-member, but must contain Os derived from a continental/aeolian, cosmic, volcanic, or anthropogenic source. Rivers, groundwater discharge, and potentially submarine hydrothermal fluids are regarded as the major sources of Os to seawater (Levasseur et al., 1999; Peucker-Ehrenbrink and Ravizza, 2000; Paul et al., 2010; Stein and Hannah, 2014). Aeolian dust, cosmic dust, and volcanic aerosols probably constitute a minor fraction of the total Os input to seawater (Peucker-Ehrenbrink and Ravizza, 2000), but anthropogenic inputs are currently having a major impact on the Os geochemical cycle (Chen et al., 2009; Rauch et al., 2010). Below, we describe the flux and isotopic composition of each Os source to seawater (Fig. 1).

2.2.1. Rivers and groundwater: sources of radiogenic Os

During partial melting in the upper mantle, Os behaves as a compatible element with respect to mantle minerals, whereas Re is moderately incompatible. Hence, the partial melts and thus the crustal rocks crystallized from them have higher Re/Os ratios than the mantle (Shirey and Walker, 1998). Over time, the radioactive decay of ^{187}Re to ^{187}Os results in higher ^{187}Os/^{188}Os ratios for the crust relative to the mantle. Oxidative

weathering of old continental crust thus releases radiogenic Os that can be transported by rivers and groundwater to the oceans.

Riverine Os concentrations range from 4.6 to 52.1 pg/kg (average = 7.9 pg/kg) based on analysis of water samples from 17 rivers worldwide (representing 35% of discharge); thus, river and seawater Os concentrations overlap (Fig. 1; Levasseur et al., 1999). Indeed, the ratio of dissolved Os to particulate Os is only ~ 0.1, indicating that only a small amount of Os is delivered to the oceans in dissolved form (Sharma, 2012). By assuming a riverine flux to the ocean equal to 37,400 km^3/yr (Berner and Berner, 1987), Levasseur et al. (1999) calculated a total Os riverine flux of 295 kg/yr. Similarly, Peucker-Ehrenbrink and Ravizza (2000) assumed an overall average Os concentration of 9.1 pg/kg for rivers, which corresponds to an estimate of ~ 350 kg/yr for the total Os riverine flux. As noted by Sharma et al. (2007a), additional studies of rivers (e.g., Huh et al., 2004; Chen et al., 2006; Gannoun et al., 2006; Sharma et al., 2007a; Turekian et al., 2007) do not appreciably change these averages.

Oxburgh (2001) pointed out that some rivers with smaller water fluxes can contain much higher Os concentrations (> 30 pg/kg) whereas rivers with larger fluxes have Os concentrations similar to that of seawater. However, the Os dataset for small rivers is small. If smaller rivers have a higher average Os concentration than large rivers, then the riverine input flux of Os to the oceans is potentially underestimated. Another factor affecting estimates of the riverine Os flux to the oceans is that a portion of the Os (perhaps ~ 15%) may be retained in estuaries, particularly in Arctic and temperate regions

(Turekian et al., 2007). Taking the effect of estuaries into consideration, Sharma et al. (2007) and Georg et al. (2013) estimated 284 kg/year and 267 kg/year, respectively, for the riverine Os flux.

The $^{187}Os/^{188}Os$ of modern rivers spans a large range (1.1−2.9) and is suggested to have an average of ~ 1.2–1.5 (Levasseur et al., 1999; Peucker-Ehrenbrink, 2002; Sharma et al., 2007a; Sharma, 2012; Georg et al., 2013; Fig. 1). If the upper end of this estimate is correct, then the riverine flux would be more radiogenic than average upper continental crust (0.8–1.4; Esser and Turekian, 1993; Peucker-Ehrenbrink and Jahn, 2001; Hattori et al., 2003; Chen et al., 2016), which can be reconciled by preferential release of radiogenic ^{187}Os during oxidative weathering of Re- and Os-rich crustal sulfide minerals (particularly molybdenite and pyrite) and ORM (Cohen et al., 1999; Stein et al., 2001; Hannah et al., 2004; Morelli et al., 2004; Golden et al., 2013; Dubin and Peucker-Ehrenbrink, 2015). Crustal sulfide minerals may be the most important reservoir of Os given that ORM are estimated to contain only ~ 5–10% of the crustal Os reservoir (Dubin and Peucker-Ehrenbrink, 2015). However, the average $^{187}Os/^{188}Os$ of the crustal sulfide Os reservoir is poorly constrained, and thus the river average $^{187}Os/^{188}Os$ has a large uncertainty.

Groundwater discharge of Os to the oceans may be an important source of Os. Groundwater samples from the Bengal plain (Asia) are characterized by high Os concentrations of 16.9−191.5 pg/kg (average = 70 pg/kg) and radiogenic $^{187}Os/^{188}Os$ ranging from 0.96 to 2.79 (Paul et al., 2010). Assuming the average Os concentration of

groundwater from the Bengal Basin (70 pg/kg) is representative for that of global groundwater, and the total groundwater discharge to the ocean of 2600 km^3/yr (Berner and Berner, 1987; Zektser and Loaiciga, 1993), then the total groundwater Os flux may be ~ 182 kg/yr, which potentially represents the second largest Os input to the oceans after rivers. Because the role of groundwater discharge on the marine Os budget remains poorly constrained, the above estimate is tentative.

2.2.2. Seafloor hydrothermal systems and cosmic dust: sources of unradiogenic Os

In contrast to rivers and groundwater, high-temperature hydrothermal fluids on the seafloor supply unradiogenic mantle-derived Os to the oceans ($^{187}Os/^{188}Os$ ~ 0.13) whereas low-temperature hydrothermal fluids are a source of more radiogenic Os ($^{187}Os/^{188}Os$ ~ 0.88; Ravizza et al., 1996; Shirey and Walker, 1998; Peucker-Ehrenbrink and Ravizza, 2000; Cave et al., 2003; Sharma et al., 2000, 2007b; Fig. 1). The Os concentrations of these hydrothermal fluids range from 3 to 100 pg/kg. Recently, Georg et al. (2013) estimated high-temperature and low-temperature hydrothermal fluxes of ~ 30 kg/yr and ~ 19−56 kg/yr, respectively. Hence, basalt-dominated seafloor hydrothermal systems are minor sources of Os to the oceans compared with rivers (and possibly groundwater). Ultramafic-hosted hydrothermal systems at slow- and ultraslow-spreading ridges may provide larger fluxes of Os to seawater given that peridotites are enriched in Os by 2–3 orders of magnitude compared with basalts (e.g., Shirey and Walker, 1998), but direct measurement of Os concentrations in fluids from ultramafic-hosted systems

have not been made (Cave et al., 2003; Sharma et al., 2007b). If confirmed, then the flux of hydrothermal Os to the oceans is strongly controlled by the host lithology at seafloor spreading centers.

Cosmic dust is characterized by high Os concentrations of 0.270−8.8 mg/kg and unradiogenic $^{187}Os/^{188}Os$ of ~ 0.13 (Luke and Allègre, 1983; Sharma et al., 1997; Walker et al., 2002). The total extraterrestrial flux of Os to the oceans, assuming complete dissolution of cosmic dust, has been estimated at 7 to 60 kg/year (Peucker-Ehrenbrink and Ravizza, 2000; Dalai and Ravizza, 2006; Sharma et al., 2007b), with a value of ~ 19 kg/year used by Georg et al. (2013). However, it is not known if all Os from cosmic dust is dissolved into the oceans (Sharma et al., 2007b), raising the possibility that the cosmic Os flux is overestimated.

Subaerial exposure and weathering of mafic and especially ultramafic Os-rich rocks and juvenile crust (enriched in Os: 1−10 μg/kg) will also release unradiogenic Os ($^{187}Os/^{188}Os$ ~ 0.13) to the oceans, but is not an important process today (Fig. 1; Crocket, 1979; Shirey and Walker, 1998; Saal et al., 2001). Such a flux may have been important in the past, however, such as during the emplacement and weathering of large igneous provinces (e.g., Turgeon and Creaser, 2008).

2.2.3. Other sources of osmium to seawater

Aeolian dust contains Os concentrations of 19−100 ng/kg and radiogenic $^{187}Os/^{188}Os$ similar to the upper continental crust (Fig. 1; Esser and Turekian, 1993;

Peucker-Ehrenbrink and Jahn, 2001; Hattori et al., 2003). Peucker-Ehrenbrink and Ravizza (2000) estimated the aeolian dust flux to the oceans at ~ 28 kg/year. Volcanic aerosols have Os concentrations of 0.03−1 μg/kg and variable $^{187}Os/^{188}Os$ of 0.12−0.60 (Krähenbühl et al., 1992; Sims et al., 2005; Yudovskaya et al., 2008). The flux of Os from volcanic aerosols is poorly constrained, but rainwater associated with ocean island volcanism is not enriched in Os, suggesting that volcanic aerosols are not an important source of Os to seawater (Sharma et al., 2007b).

Anthropogenic Os in precipitation ($^{187}Os/^{188}Os$ = 0.16–0.48) appears to have decreased the $^{187}Os/^{188}Os$ of surface seawater from ~ 1.05 to ~ 0.95, with the flux of anthropogenic Os to the oceans estimated to be ~ 2391 kg/year (Chen et al., 2009). Hence, anthropogenic inputs (e.g., high demand for automobile catalytic converters, increased fossil fuel combustion) are currently affecting the Os marine geochemical cycle at a global scale (Chen et al., 2009; Rauch et al., 2010). It is less clear, however, to what extent anthropogenic Os in precipitation has influenced estimates of the riverine and groundwater fluxes of Os to the oceans.

2.3. Osmium sinks and their burial rates in modern marine environments

The Os sinks in the modern ocean are anoxic sediments underlying suboxic and anoxic bottom waters, as well as ferromanganese (Fe-Mn) crusts/nodules, carbonates, and pelagic/hemipelagic sediments deposited from oxygenated bottom waters.

2.3.1. Anoxic sediments

Dissolved Os species become insoluble and are removed from seawater into anoxic sediments underlying suboxic and anoxic bottom waters (Levasseur et al., 1998; Selby and Creaser, 2003; Yamashita et al., 2007). Here, we use the term "suboxic" to denote environments with mildly or weakly oxygenated bottom waters and limited O_2 penetration (< 1 cm) below the sediment-water interface. Several factors may influence the Os removal process, such as hydrolysis, sulfur complexation, and organic complexation, but these processes are not well understood (Yamashita et al., 2007). Osmium may be removed first as Os(IV), followed by further reduction to Os(III) in anoxic sediments (Yamashita et al., 2007). In general, the Os concentrations of pyrite nodules from ORM are significantly lower than those in bulk ORM, suggesting that removal of Os from sediment pore waters largely occurs before the formation of diagenetic pyrite nodules (Cohen et al., 1999). However, syn-depositional to early diagenetic pyrites are known to contain high concentrations of Os (Hannah et al., 2004), so both organic matter and sulfide minerals can be significant hosts for Os in ORM.

Authigenic enrichments of Os occur in sediments underlying suboxic and anoxic (including euxinic) waters. It is not known if Os removal can efficiently occur within an anoxic water column, or mostly takes place below the sediment-water interface. Authigenic Os enrichments are known to occur in ORM without Mo enrichment, suggesting that Os burial in sediments does not simply scale with dissolved H_2S availability as is generally the case for Mo (Erickson and Helz, 2000; Morford et al.,

2005; Xu et al., 2014; Scott and Lyons, 2012). Osmium burial fluxes for sediments underlying suboxic bottom waters (oxygen minimum zones) in continental margin settings range from 2 to 12 pg/cm^2/yr (Ravizza and Turekian, 1992; Dean, 2006; Paquay and Ravizza, 2012). By comparison, average Os burial fluxes into sediments underlying euxinic bottom waters in the weakly restricted Saanich Inlet and moderately restricted Cariaco Basin are not significantly different at 16 pg/cm^2/yr (Poirier, 2006) and 6−10 pg/cm^2/yr (over the past 15 kyr; Oxburgh et al., 2007), respectively (Table 1).

Lower Os burial rates (2.0−3.1 pg/cm^2/yr) are observed in the euxinic sediments of the more restricted Black Sea (Ravizza et al., 1991), suggesting that the Os burial flux in anoxic sediments is influenced by the degree of basin restriction from the open ocean. Although direct measurement of bottom water Os concentrations in anoxic basins has not yet been done, it is possible that the lower Os burial fluxes in the Black Sea reflect lower bottom water Os concentrations because of slow rates of deep-water renewal. A positive correlation between bottom water concentrations and authigenic metal enrichment in the sediments of modern anoxic basins has been shown for some redox-sensitive metals like Mo and Zn (Algeo and Lyons, 2006; Scott et al., 2013). Despite the greater degree of water restriction and lower Os burial rate in the Black Sea, however, the sediments have higher Os concentrations and Os/TOC ratios relative to sediments in the less restricted Saanich Inlet and Cariaco Basin (Ravizza et al., 1991; Poirier, 2006; Oxburgh et al., 2007; Paquay and Ravizza, 2012). Hence, other factors (e.g., sedimentation rates, organic

matter characteristics, water column pH) likely influence the Os concentrations of organic-rich sediments in semi-restricted basins.

2.3.2. Oxic sediments

In oxygenated marine environments, higher Os concentrations are found in Fe-Mn crusts and nodules (10^2–10^4 pg/g; Koide et al., 1991; Burton et al., 1999; Peucker-Ehrenbrink and Ravizza, 2000; McDaniel et al., 2004) and metalliferous sediments (10–1500 pg/g; Ravizza, 1993; Peucker-Ehrenbrink et al., 1995). Generally lower Os concentrations are found in non-metalliferous carbonates and fine-grained siliciclastic muds (25–360 pg/g; Ravizza et al., 2001; Dalai et al., 2005; Dalai and Ravizza, 2006).

Given a typical Fe-Mn crust growth rate of 1–10 mm/Ma and bulk density of 2 g/cm^3 (Burton et al., 1999), the accumulation rate of Fe-Mn crusts is (0.2–2) × 10^{-6} g/cm^2/yr, which agrees with measurements of Mn sedimentation rate in deep-sea pelagic sediments and nodules ([0.1–3.4] × 10^{-6} g/cm^2/yr; Bender et al., 1970). Combined with Os concentrations of 10^2–10^4 pg/g in Fe-Mn crusts and nodules, the average Os burial rate in this oxic setting is 6 × 10^{-4} pg/cm^2/yr (geometric mean, Table 1) Hence, Fe-Mn crusts and nodules are not a significant sink in the marine Os budget.

Other types of seafloor sediments in oxic settings are associated with higher Os burial rates. For example, Paquay and Ravizza (2012) calculate Os burial fluxes of 0.03–0.09 pg/cm^2/yr for pelagic carbonates from ODP Site 849 in the Eastern Equatorial Pacific. Similarly, hemipelagic muds from the Sea of Japan, deposited after the last

glacial maximum, record Os burial rates of 0.05–0.11 pg/cm^2/yr. These burial rates are a few orders of magnitude greater than for Fe-Mn crusts and nodules. Overall, the Os burial flux in oxic settings is not well understood and more studies are required to further refine the estimate for Os flux into oxic sinks.

2.4. Oceanic Os mass balance and seawater residence time

Previous estimates of the residence time for Os in seawater ranged between ~ 5 and 54 kyr, which is shorter than the residence times of many other redox-sensitive trace metals (e.g., 400–500 kyr for Mo and U; Ku et al., 1977; Dunk et al., 2002; Miller et al., 2011) but longer than the modern ocean mixing time (1−2 kyr) (Sharma et al., 1997; Levasseur et al., 1998, 1999; Woodhouse et al., 1999; Oxburgh, 2001; Oxburgh et al., 2007; Paquay and Ravizza, 2012; Georg et al., 2013). The large uncertainty in the seawater Os residence time is not surprising given that large uncertainties remain for Os input/output fluxes (Levasseur et al., 1998, 1999; Peucker-Ehrenbrink and Ravizza, 2000; Oxburgh, 2001; Oxburgh et al., 2007; Paul et al., 2010; Hannah and Stein, 2012; Georg et al., 2013).

A non-anthropogenic Os isotope mass balance to explain the $^{187}Os/^{188}Os$ of modern deep seawater (~1.05) can be expressed by the following equation:

$$^{187}Os/^{188}Os_{seawater} = (^{187}Os/^{188}Os_{rivers}\ f_{rivers} + {}^{187}Os/^{188}Os_{groundwater}\ f_{groundwater} + {}^{187}Os/^{188}Os_{high\text{-}T\ hydrothermal}\ f_{high\text{-}T\ hydrothermal} + {}^{187}Os/^{188}Os_{low\text{-}T\ hydrothermal}\ f_{low\text{-}T\ hydrothermal} + {}^{187}Os/^{188}Os_{cosmic}\ f_{cosmic} + {}^{187}Os/^{188}Os_{aeolian}\ f_{aeolian} + {}^{187}Os/^{188}Os_{volcanic}\ f_{volcanic}) / f_{total}$$

where f = flux of Os from each source. Despite the large uncertainties on essentially all fluxes of Os to the oceans as well as the average isotopic compositions of rivers, groundwater, low-temperature hydrothermal fluids, and aeolian dust, it is noted that the modern deep ocean $^{187}Os/^{188}Os$ can be obtained using current estimates (e.g., Fig. 2a). However, this solution uses minimum estimates for average riverine and aeolian $^{187}Os/^{188}Os$, and other mass-balance solutions can easily be visualized. As just one example, if the high-temperature hydrothermal flux of Os to the oceans is found to be higher than previously estimated (i.e., an additional Os contribution from ultramafic-hosted hydrothermal systems), then more radiogenic river, groundwater, and/or aeolian dust would be required to explain the deep seawater $^{187}Os/^{188}Os$ of 1.05 (e.g., Fig. 2b).

Given that anoxic settings cover ~ 0.35% of the total seafloor and considering the range of Os burial rates in anoxic basins (2–16 pg/cm^2/yr), the total Os burial flux for this sink today is between 25 and 202 kg/yr (Table 1). Assuming that suboxic settings cover ~ 6.00% of the total seafloor and are associated with burial rates of 2–12 pg/cm^2/yr, significantly higher total Os burial fluxes of 433 to 2600 kg/yr are calculated (Table 1). Using the Os burial rates of 0.05–0.11 pg/cm^2/yr from the Sea of Japan and Eastern Equatorial Pacific and assuming the oxic sink covers ~ 93.65% of the total seafloor, we calculate a total burial rate of ~ 170–372 kg/yr for this sink. This estimate is probably a maximum for the total Os burial flux into oxic sediments given the much slower burial rates into Fe-Mn crusts and nodules. Considering the minor fraction of the seafloor

covered by suboxic and anoxic sinks, the disproportionately high burial fluxes of Os into these sinks demonstrate the redox-sensitive nature of Os.

Our estimates of the Os sink fluxes poses a conundrum – the range of possible total Os burial fluxes (oxic + suboxic + anoxic sinks) largely exceeds the estimated total Os input flux into the oceans (nearly 600 kg/yr; Fig. 2a). It is possible to balance the oceanic Os budget when the lower end of the range of suboxic burial fluxes is used. Alternatively, the total Os input flux to the oceans may be underestimated, in which case the larger burial sink fluxes (particularly for the suboxic sink) can be accommodated. More studies are required to better constrain the representative Os burial rate of each sink and the oceanic mass balance of Os.

3. METHODS

3.1. Compilation of ^{192}Os concentrations

We define Archean, pre-Ediacaran Proterozoic, and Ediacaran-Phanerozoic time bins to determine if there is any evidence that coupled first-order increases in the Os concentrations and initial $^{187}Os/^{188}Os$ (= local seawater $^{187}Os/^{188}Os$ at the site of deposition) of ORM occurred over time, as might be expected due to increased atmosphere-ocean oxygenation. All data used in our Os compilation were derived from the published literature. Osmium and total organic carbon (TOC) contents were compiled from ~ 1000 samples of ORM (Table A.1). We passed the Os data through a quality filter to exclude oxygenated sediments, obvious examples of sediments deposited in non-

marine basins based on paleogeographic and sedimentological information, sediments deposited in highly restricted basins, and sediments significantly affected by post-depositional disturbance. Geologically reasonable and precise Re-Os ages are available for most intervals, and suggest negligible or minor post-depositional disturbance of ORM by weathering, metamorphism, and subsurface hydrothermal fluid flow.

Our compilation efforts targeted samples representing local anoxic sediment conditions, with overlying bottom waters that are suboxic to anoxic. This approach is justified because of the nearly similar Os burial rates in modern suboxic and anoxic/euxinic basins (Table 1). For all pre-modern samples in the compilation, Re concentration data are available to serve as an independent indicator of local redox conditions at the site of deposition. In modern continental margin environments where bottom waters are well-oxygenated and the depth of O_2 penetration below the sediment-water interface is > ~1 cm, negligible authigenic Re enrichments are typically observed in sediments (Crusius et al., 1996; Morford and Emerson, 1999; Morford et al., 2005, 2012). By contrast, if the bottom waters are only mildly oxygenated or anoxic, then the depth of O_2 penetration below the sediment-water interface is typically small (< ~1 cm) or negligible, resulting in Re concentrations in organic-rich sediments that are higher than the average Re concentration of the upper continental crust (198 pg/g from Peucker-Ehrenbrink and Jahn, 2001; 230−370 pg/g from Dubin and Peucker-Ehrenbrink, 2015; 400 pg/g from Esser and Turekian, 1993). For our compilation, we rejected Os data from

samples with Re concentrations < 5 ng/g because such low concentrations reflect deposition from well-oxygenated bottom waters.

For some intervals, independent evidence for sediment anoxia is also provided by Mo enrichments and sedimentary Fe speciation data. Molybdenum concentrations higher than that of the average upper crust (1.5 µg/g; McLennan, 2001) indicate the presence of dissolved hydrogen sulfide in sediment pore waters, and concentrations >100 µg/g point to water column euxinia (Scott and Lyons, 2012). The ratio of biogeochemically highly reactive Fe to total Fe (Fe_{HR}/Fe_T) in sediments deposited in anoxic marine basins typically exceeds 0.38, whereas sediments deposited in oxygenated settings have lower ratios (Raiswell and Canfield, 1998; Poulton and Raiswell, 2002; Poulton and Canfield, 2005, 2011). In addition, Fe/Al ratios greater than the average crustal value of ~ 0.5 point to anoxic bottom water conditions (Lyons and Severmann, 2006). Degree of pyritization (DOP) values (defined as $Fe_{PY}/[Fe_{PY} + Fe_{HCl}]$ where Fe_{HCl} represents the acid-soluble iron content determined from a one-minute boiling HCl extraction) that are higher than 0.45 indicate an anoxic water column (Raiswell et al., 1988, 1994; Lyons and Severmann, 2006). Table A.2 identifies intervals containing elevated Mo concentrations and Fe speciation and DOP evidence for anoxic sediment conditions, in addition to Re enrichment.

In addition to well-oxygenated conditions, a high degree of restriction between the open ocean and a local sedimentary basin can cause low Re and Os concentrations in sediments even if the overlying bottom waters are anoxic (e.g., McArthur et al., 2008).

Our Re filter helps exclude unusually low ^{192}Os concentrations from ORM deposited in highly restricted basins. Euxinic sediments in the Black Sea, however, still have Re concentrations higher than 5 ng/g (Ravizza et al., 1991). Hence, it is likely that some Os data from ancient semi-restricted basins are included in our compilation. Although we cannot rectify this issue, it likely affects all time bins to some extent, such that first-order differences in the Os data between time bins arising from other factors (such as changes in atmosphere-ocean oxygenation) may still be discernable (as was the case for the compilations of Mo and U concentrations in ORM; Scott et al., 2008; Partin et al., 2013a; Reinhard et al., 2013).

In addition to ^{192}Os concentrations, we also present a compilation of ^{192}Os/TOC ratios to (1) explore the extent to which ^{192}Os and TOC contents are correlated in ORM, and (2) check for any effect of variable organic carbon enrichment on the temporal trends of ^{192}Os enrichments in ORM. As a further quality control measure, we rejected samples with low total organic carbon (TOC) contents of less than 0.5 wt.% to avoid spuriously high ^{192}Os/TOC ratios.

Osmium concentrations in ORM reflect syn-depositional Os plus radiogenic ^{187}Os produced by *in-situ* radioactive decay of ^{187}Re between the time of deposition and today. Hence, the most abundant non-radiogenic Os isotope in nature (^{192}Os) is used to represent depositional Os concentrations (the average ^{192}Os concentration of the upper continental crust is ~ 12−24 pg/g based on an average total Os concentration of 30−60 pg/g; Esser and Turekian, 1993; Peucker-Ehrenbrink and Jahn, 2001; Hattori et al., 2003; Chen et al.,

2016). Some publications provide the ^{192}Os concentrations of samples directly, but in many cases, only the total Os concentration and present-day $^{187}Os/^{188}Os$ isotope ratios are provided. In these cases, we calculated the ^{192}Os concentration of a sample using its total Os concentration and present-day $^{187}Os/^{188}Os$ isotope ratio, the fixed (constant) isotope ratios for other Os isotopes ($^{184}Os/^{188}Os = 0.001383$; $^{186}Os/^{188}Os = 0.11983$; $^{188}Os/^{188}Os = 1$; $^{189}Os/^{188}Os = 1.21965$; $^{190}Os/^{188}Os = 1.98379$; $^{192}Os/^{188}Os = 3.08261$), and the sample's calculated atomic weight (which varies according to present-day $^{187}Os/^{188}Os$).

3.2. Compilation of Re-Os ages and initial $^{187}Os/^{188}Os$

For the seawater $^{187}Os/^{188}Os$ record, we compiled initial $^{187}Os/^{188}Os$ isotope ratios from Re-Os isochron regressions of ORM that yield geologically reasonable Re-Os depositional ages. Most publications report Re-Os ages and initial $^{187}Os/^{188}Os$ isotope ratios using the regression algorithm of the Microsoft Excel add-in program *Isoplot* (Ludwig, 2011). For the few exceptions, we recalculated the Re-Os age and the initial $^{187}Os/^{188}Os$ value using *Isoplot*. A Re-Os age is assumed to be reasonable if it has a Mean Square of Weighted Deviates (MSWD) close to 1 because there are multiple examples of a concordant Re-Os ORM age (with low MSWD) and a U-Pb zircon age from the same stratigraphic unit or for the same geological timescale boundary (e.g., Selby and Creaser, 2005; Anbar et al., 2007; Selby, 2007; Turgeon et al., 2007; Xu et al., 2009). If a Re-Os age has a higher MSWD (> 1), but is known to be reasonable based on independent geochronological constraints, then it is considered acceptable. Such ages may have higher

MSWD because of variations in the initial $^{187}Os/^{188}Os$ of ORM due to changes in seawater $^{187}Os/^{188}Os$ over the stratigraphic interval sampled for geochronology. However, Os samples are excluded in the compilation if negative initial $^{187}Os/^{188}Os$ ratios are yielded from isochrons. If a Re-Os ORM age is erroneously young or old based on independent age constraints, then its Os data were not included in the compilation. The vast majority of stratigraphic intervals in our compilation have geologically reasonable Re-Os ages with MSWD < 10 (and many near ~1). Hence, post-depositional processes are highly unlikely to have adversely affected the temporal tends in the ^{192}Os, $^{192}Os/TOC$, and initial $^{187}Os/^{188}Os$ compilations.

3.3 Statistical Analyses

Histograms for individual ^{192}Os data points in each time bin are characterized by long tails towards larger concentrations, indicating that the Os data do not follow normal distributions (Fig. 3a). This observation suggests that parametric analysis (e.g., Student's t-test) cannot be used to validate a statistical difference between any two time bins.

A time bin average based on individual data points would be biased towards samples with extremely high ^{192}Os concentrations and formations / time points with a large number of Os data points (Fig. 3a). Hence, we re-assigned individual Os values rounded to the nearest 5 Ma (Table A.2) and calculated the average ^{192}Os concentration and $^{192}Os/TOC$ ratio of each 5 Ma time point. Using these averages for 5 Ma time points, we calculated averages, standard deviations, and medians of ^{192}Os concentrations,

^{192}Os/TOC ratios, and initial ^{187}Os/^{188}Os ratios for each time bin (Table 2). This procedure greatly reduces the biases and yields more representative ^{192}Os data. Histograms for ^{192}Os time points in each time bin (Fig. 3b) suggest that these Os time point data are not so strongly skewed, but nevertheless are still not normally distributed.

Therefore, to analyze Os data in each time bin, a bootstrapping method (Efron, 1979) was applied, as used in a previous Os study (Dubin and Peucker-Ehrenbrink, 2015). This technique relies on random sampling, and provides valuable estimations of a data distribution when the realistic sample distribution is unknown. Specifically, 10,000 ^{192}Os data subsets are generated for each time bin. Each of the 10,000 subsets for each time bin contain the same number of data points as the corresponding time bins. Data points in each ^{192}Os subsets of a time bin are randomly selected from the time point averages of that time bin using the RANDBETWEEN function in the Microsoft Excel. This function allows picking data from all the time point averages of a time bin, whether or not the time point averages have been previously selected. For instance, the filtered Archean ^{192}Os database is (70.5, 129.5, 24.5, 346.5) (Table 2); using the RANDBETWEEN function in the Microsoft Excel, a new subset of Archean ^{192}Os could be (129.5, 346.5, 129.5, 24.5) and other possibilities are likely such as (24.5, 129.5, 70.5, 70.5). As the median is a more robust statistic than the mean for a non-Gaussian data set, a median is calculated for each subset. For each of the time bins, we calculated a mean of the 10,000 ^{192}Os bootstrap medians, along with a 95% confidence interval (Table 3). This

exercise was not done for ^{192}Os/TOC ratios, however, because ^{192}Os-TOC relationships in ORM were found to be complex (see section 5.1).

4. RESULTS

The filtered ^{192}Os, ^{192}Os/TOC, and initial ^{187}Os/^{188}Os compilations are presented in Fig. 4, Table A.1, and Table A.2. The ^{192}Os concentrations in the compilation span three orders of magnitude and range between 13 pg/g and 26,592 pg/g, whereas ^{192}Os/TOC ratios range between 4 pg/g/wt.% and 1831 pg/g/wt.%. The average ^{192}Os concentrations of ORM for the Archean, pre-Ediacaran Proterozoic, and Ediacaran-Phanerozoic time bins based on ^{192}Os time points (rounded to the nearest 5 Ma, Table A.2) are 143 ± 143 pg/g (1SD, median = 100, n = 4), 111 ± 96 pg/g (1SD, median = 82, n = 13), and 372 ± 616 pg/g (1SD, median = 155, n = 33), respectively (Table 2). For all time bins, the average ^{192}Os concentrations are elevated above the average value of the upper continental crust (12–24 pg/g) by a factor of at least four. Average ^{192}Os/TOC ratios for the Archean, pre-Ediacaran Proterozoic, and Ediacaran-Phanerozoic time bins are 65 pg/g/wt.% (median = 65, n = 1), 32 ± 16 pg/g/wt.% (1SD, median = 27, n = 6), and 97 ± 90 pg/g/wt.% (1SD, median = 70, n = 21), respectively (Table 2). Initial ^{187}Os/^{188}Os ratios from Re-Os isochron regressions range between 0.06 ± 0.09 and 1.26 ± 0.22 (Table A.2). Average initial ^{187}Os/^{188}Os ratios for the Archean, pre-Ediacaran Proterozoic, and Ediacaran-Phanerozoic time bins are 0.18 ± 0.04 (1SD, median = 0.18, n = 2), 0.46 ±

0.29 (1SD, median = 0.43, n = 24), and 0.64 ± 0.32 (1SD, median = 0.60, n = 25), respectively (Table 2).

The means of 10,000 ^{192}Os bootstrap medians (with replacement) and associated 95% confidence intervals (in brackets) for the Archean, pre-Ediacaran Proterozoic, and Ediacaran-Phanerozoic time bins based on time points are 157 pg/g (25, 347), 88 pg/g (35, 159), and 187 pg/g (91, 329), respectively (Table 3). The calculated median values of each time bin (Table 2) fall in the corresponding 95% bootstrapped confidence intervals (Table 3) and display a good consistency. Hence, for the rest of this study, the means of 10,000 ^{192}Os bootstrap medians and 95% confidence intervals are used to determine if there are statistically meaningful differences in ^{192}Os between two time bins.

Two groups of anomalously high ^{192}Os enrichments can be readily identified from the ^{192}Os and ^{192}Os/TOC compilations and their corresponding histograms (Fig. 3). One group is associated with highly radiogenic initial ^{187}Os/^{188}Os ratios (Ediacaran and Cambrian Periods) whereas the other group is associated with highly unradiogenic initial ^{187}Os/^{188}Os ratios (Mesozoic and early Cenozoic Eras). Excluding these anomalously high enrichments, the average ^{192}Os concentration, ^{192}Os/TOC ratio, and initial ^{187}Os/^{188}Os ratio for the Ediacaran-Phanerozoic time bin is 166 ± 148 pg/g (1SD, median = 106, n = 25), 66 ± 71 pg/g/wt.% (1SD, median = 38, n = 15), and 0.71 ± 0.26 (1SD, median = 0.65, n = 18), respectively (Table 2). The mean of 10,000 ^{192}Os bootstrap medians (with replacement) for the Ediacaran-Phanerozoic time bin (with no anomalous groups) is 112 pg/g with a 95% confidence interval of (72, 168) (Table 3).

5. DISCUSSION

5.1. Relationship Between ^{192}Os and TOC contents in ORM

We first explore the relationship between ^{192}Os concentrations and TOC contents in ORM. The use of ^{192}Os/TOC ratios in ORM as a proxy for inferring the presence or absence of temporal trends in seawater Os concentrations (i.e., between the Archean, pre-Ediacaran Proterozoic, and Ediacaran-Phanerozoic time bins) may be a better approach than using raw ^{192}Os concentrations. This would be true if it can be shown that (1) Os is associated with organic matter, (2) a relationship exists between ^{192}Os concentrations and TOC contents in ORM, and (3) the ^{192}Os/TOC ratio scales with bottom water Os concentrations. Osmium concentrations in organic matter that was chemically separated from ORM are known to be significantly higher than the Os concentration of bulk ORM samples, thus demonstrating that organic matter can be a major host of Os in ORM (Ripley et al., 2001; Selby and Creaser, 2003). If organic matter is the major host of Os, then the ^{192}Os and TOC contents from a single stratigraphic interval of ORM should be well-correlated, provided the Os concentration of overlying bottom waters, local bottom water redox conditions, and type of organic matter delivered to sediments (a current knowledge gap) were all constant. Good correlations are indeed found between ^{192}Os concentrations and TOC contents in approximately one-third of ORM localities ($R^2 > 0.7$, Fig. 5), implying organic matter is a major host of Os for some shales. Normalizing ^{192}Os

concentrations to TOC contents would also have the advantage of reducing the effect of variable ORM sedimentation rates, which affects raw ^{192}Os concentrations.

Poor correlations are observed, however, between ^{192}Os concentrations and TOC contents for many stratigraphic intervals in the compilation (Fig. 5). Decoupled ^{192}Os-TOC systematics for ORM within a single stratigraphic interval are expected if there were a significant variation in the ^{192}Os concentrations of bottom waters or a major change in the composition of organic matter being delivered to the sediments (Rooney et al., 2010). A good example is provided by the Touirist Formation (Fig. 5ab). Two discrete stratigraphic sub-intervals within the Touirist Formation each yield a good correlation between ^{192}Os and TOC contents (solid line, R^2 = 0.90 to 0.94). However, each interval has a different ^{192}Os-TOC slope, suggesting that local depositional conditions were not the same for those two intervals (Rooney et al., 2010). Combining the intervals in the Touirist Formation thus results in a poor correlation between ^{192}Os and TOC contents (dashed line, R^2 = 0.05).

Additional complications for the use of ^{192}Os/TOC ratios are that the molecular composition of the organic host phase(s) for Os in ORM is poorly understood. Furthermore, the poor ^{192}Os-TOC correlations for many ORM implies that the uptake of Os in the ORM may be influenced by other factors such as the Os concentrations in the water column, local bottom water redox conditions, and type of organic matter. If suitable organic substrates are not available during deposition, Os will likely be incorporated into

sulfide minerals (e.g., Hannah et al., 2004), in which case the relationship between ^{192}Os and TOC contents in ORM may not be straightforward.

A final possible complication for interpreting temporal trends in the trace metal concentrations of ORM is that these rocks are deposited predominantly in continental margin environments rather than in open ocean settings (whose record has been largely destroyed by subduction of oceanic lithosphere). At any one time in Earth's history, sedimentary basins along continental margins (intracratonic basins or epicontinental seas) will have different degrees of restriction from the open ocean; seawater metal concentrations are lower in more restricted basins because the rate of removal of metals to anoxic sediments exceeds rates of deepwater recharge (e.g., Algeo and Lyons, 2006; Scott et al., 2013). Hence, basin restriction will potentially lower the ^{192}Os/TOC ratios of ORM. However, this may not be true for all semi-restricted basins because the modern Black Sea has higher ^{192}Os concentrations and ^{192}Os/TOC ratios than the less restricted Saanich Inlet and Cariaco Basin (Table A.2). Although we have avoided including ORM affected by extreme basin restriction in our compilation (see section 3.1), differences in the efficiency of water exchange between local basins and the open ocean probably impact some of our data in ways we cannot rectify.

Organic-rich sediments deposited during Oceanic Anoxic Event 1a (OAE1a; ca. 120 Ma) provide an example of an increase in the ^{192}Os concentrations and ^{192}Os/TOC ratios of ORM in response to higher seawater ^{192}Os concentrations. In two stratigraphic intervals from Italy, samples with more radiogenic initial ^{187}Os/^{188}Os (calculated for each

individual sample using the depositional age and present-day isotope ratios) define good correlations between ^{192}Os and TOC contents (R^2 ~ 0.7−0.9; squares in Fig. 5f, 5g). However, those samples with unradiogenic initial $^{187}Os/^{188}Os$ (triangles in Fig. 5f, 5g) have higher ^{192}Os concentrations and plot to the right of the samples with more radiogenic initial $^{187}Os/^{188}Os$. Hence, the higher ^{192}Os enrichments during OAE1a was probably caused by a transient increase of magmatic-hydrothermal Os inputs to seawater during the emplacement of a large igneous province (LIP; the Ontong Java Plateau) in the Pacific Ocean (Fig. 5f, 5g; Tejada et al., 2009; Bottini et al., 2012). A similar relationship between ^{192}Os concentrations and initial $^{187}Os/^{188}Os$ ratios was also observed for ORM deposited during OAE2 (ca. 93.5 Ma) at a time of LIP emplacement (the Caribbean-Colombian Igneous Plateau, Turgeon and Creaser, 2008; Du Vivier et al., 2014, 2015).

Overall, correlations between ^{192}Os and TOC content suggest that organic matter is a major Os host for some shales, but not the only one (Fig. 5). Os enrichment in ORM must be controlled by other factors (such as bottom water pH conditions, temperatures, types of organic matter) that are currently poorly understood. In addition, there is currently no direct evidence to document a positive correlation between dissolved Os concentrations and sediment ^{192}Os/TOC ratios (or sediment ^{192}Os concentrations). Hence, ^{192}Os/TOC ratios cannot provide robust evidence to reflect changes of the seawater Os reservoir through time. Nevertheless, the mean of 10,000 ^{192}Os bootstrap median values and their 95% confidence intervals for ORM from the Archean, pre-Ediacaran

Proterozoic, and Ediacaran-Phanerozoic time bins should contain some information about the average sedimentary Os reservoir during each time bin.

5.2. Temporal trends in ^{192}Os concentrations and initial ^{187}Os/^{188}Os during the past three billion years

Temporal trends in initial ^{187}Os/^{188}Os reveal first-order changes from generally unradiogenic seawater ^{187}Os/^{188}Os in the Archean (0.18 ± 0.04, 1SD, median = 0.18, n = 2; Table 2) towards more radiogenic seawater ^{187}Os/^{188}Os during the Ediacaran-Phanerozoic (0.64 ± 0.32, 1SD, median = 0.60, n = 25; Table 2). These correspond to increasing oxygenation on the Earth's surface (Fig. 4c) (Hannah et al., 2004; Kendall et al., 2009b; van Acken et al., 2013; Sperling et al., 2014; Stein and Hannah, 2014) and more radiogenic continental crust because of in-growth of radiogenic ^{187}Os from radioactive decay of ^{187}Re (e.g., Hannah and Stein, 2012).

In the Archean and early Paleoproterozoic, seawater ^{187}Os/^{188}Os is commonly indistinguishable from the unradiogenic mantle-extraterrestrial end-member, indicating a limited riverine flux of radiogenic crustal Os to seawater in a poorly oxygenated atmosphere-ocean system (Fig. 4c). One exception is a slightly higher initial ^{187}Os/^{188}Os (0.34 ± 0.19) from the ca. 2.5 Ga Mt. McRae Shale (western Australia) which, along with Re and Mo enrichments (Anbar et al., 2007), was interpreted as evidence for a transient whiff of photosynthetic O_2 production and accumulation that increased radiogenic Os inputs to the late Archean Hamersley basin (Kendall et al., 2015a). Subsequently, the

GOE, from 2.4 to 2.1 Ga, marks the appearance of the first relatively oxygenated conditions in Earth's history with the advent of oxygen-producing cyanobacteria (e.g., Lyons et al., 2014). Due to a lack of Os data, only one example characterized by unradiogenic $^{187}Os/^{188}Os$ is currently available for the GOE, which could be associated with the local depositional environment (e.g., a mafic/ultramafic provenance).

The next instance of seawater $^{187}Os/^{188}Os$ that is statistically higher than the mantle-extraterrestrial baseline occurs in the Mesoproterozoic, consistent with permanent establishment of a radiogenic Os riverine flux from the weathering of more radiogenic continental crust (Fig. 4c). However, multiple examples of unradiogenic seawater $^{187}Os/^{188}Os$ during and following the GOE in the Paleoproterozoic and Mesoproterozoic may reflect times of lower atmospheric O_2 (which limits mobility of crustal radiogenic Os and thus limits radiogenic riverine Os fluxes), proximity to local deep-sea hydrothermal inputs, and/or local subaerial weathering of juvenile crust or mafic/ultramafic rocks. Although seawater $^{187}Os/^{188}Os$ fluctuates during the Mesoproterozoic, it is not until the Neoproterozoic that seawater $^{187}Os/^{188}Os$ reaches values greater than 0.7. During the late Neoproterozoic, seawater $^{187}Os/^{188}Os$ reaches values up to ~ 1.2, indicating that a substantial riverine flux of radiogenic Os to seawater existed at least intermittently during this time (Fig. 4c). Such high seawater $^{187}Os/^{188}Os$ values may have been triggered in part by the NOE. Nevertheless, most Phanerozoic ORM, which were deposited under oxygenated atmospheric conditions, have lower initial $^{187}Os/^{188}Os$. Hence, it is likely that high crustal weathering rates during Gondwana supercontinent assembly (e.g., Shields-

Zhou and Och, 2011) and the greenhouse conditions following Snowball Earth glaciations (in the case of post-glacial ORM) also played a role in driving seawater $^{187}Os/^{188}Os$ to high values (Kendall et al., 2006, 2009b; van Acken et al., 2013; Rooney et al., 2015). The onset of Gondwana assembly could also create some restricted basins and thus radiogenic $^{187}Os/^{188}Os$ from the ORMs deposited in these basins could reflect local radiogenic riverine inputs. Nevertheless, ORMs from the Doushantuo Formation (Member IV, China) and Sheepbed Formation (Canada), which were deposited on a passive margin (Zhu et al., 2013; Kendall et al., 2015b) and a long-lived deep-water marine basin (Aitken, 1991), respectively, are characterized by radiogenic $^{187}Os/^{188}Os$ ratios (> 1.00), representing global radiogenic seawater during the late Neoproterozoic (Kendall et al., 2009b; Rooney et al., 2015).

Overall, the Ediacaran-Phanerozoic time bin shows a more radiogenic $^{187}Os/^{188}Os$ of 0.64 ± 0.32 (1SD, median = 0.60, n = 25; Table 2) compared with the record in the Archean and pre-Ediacaran Proterozoic time bins. Weathering of more radiogenic continental crust and an oxygenated atmosphere most likely are responsible for the overall higher initial $^{187}Os/^{188}Os$ ratios in Ediacaran-Phanerozoic ORM relative to pre-Neoproterozoic ORM. Large short-term fluctuations in seawater $^{187}Os/^{188}Os$ also characterize the Ediacaran-Phanerozoic time bin, reflecting changes in fluxes of radiogenic versus unradiogenic Os associated with emplacement of large igneous provinces, bolide impacts, tectonic events, lithologies of specific crustal terrains proximal to semi-restricted basins, changes in seafloor spreading rates, and climate change (Fig. 4c;

e.g., Peucker-Ehrenbrink and Ravizza, 2000; Oxburgh et al., 2007; Turgeon and Creaser, 2008; Bottini et al., 2012; Paquay and Ravizza, 2012; Xu et al., 2014; Du Vivier et al., 2014, 2015). The same geological events that affect seawater $^{187}Os/^{188}Os$ occurred in the Archean and pre-Ediacaran Proterozoic time bins as well, but significant short-term fluctuations are not observed in our compilation before the Neoproterozoic. The lack of pre-Neoproterozoic fluctuations probably results from less data, less radiogenic $^{187}Os/^{188}Os$ in crustal sources, and less riverine input to the ocean because of lower atmospheric oxygen content.

Based on the seawater $^{187}Os/^{188}Os$ record, the ^{192}Os concentrations of ORM are expected to have increased across the GOE and NOE because higher riverine Os fluxes (i.e., more oxidative mobilization of Os) and increasing ocean oxygenation favor larger sedimentary Os inventories. We test this hypothesis using the mean of 10,000 ^{192}Os bootstrap medians and its 95% confidence interval for each time bin (see Section 3.3) to determine if there is a statistically meaningful difference between the time bins (Table 3). The Archean value is 157 pg/g, with a 95% confidence interval of (25−347). Archean Os data are sparse, however; statistical analysis for this time bin is therefore highly unreliable. The mean of 10,000 ^{192}Os bootstrap medians (88 pg/g, with 95% confidence interval of 35−159) for the pre-Ediacaran Proterozoic is approximately 2 times lower than that of the Ediacaran-Phanerozoic (187 pg/g, with 95% confidence interval of 91−329), suggesting a statistically meaningful difference between the two time bins. A more oxygenated atmosphere-ocean system and weathering of more radiogenic continental

crust potentially could explain the overall, moderately higher ^{192}Os enrichments in Ediacaran-Phanerozoic ORM (Table 3).

This analysis, however, may be an oversimplification. Two groups of ORM from the Ediacaran-Phanerozoic time bin are identified by distinctive, anomalously high ^{192}Os concentrations and distinctly different initial $^{187}Os/^{188}Os$ ratios. Histograms clearly demonstrate that there are far fewer data characterized by extremely high ^{192}Os concentrations if these two groups are excluded (Fig. 3). As we show below, these anomalously high ^{192}Os concentrations are probably related to factors other than a simple change in atmosphere-ocean O_2 levels and in-growth of $^{187}Os/^{188}Os$ in the continental crust.

The first group comprises Mesozoic and Cenozoic ORM with unradiogenic initial $^{187}Os/^{188}Os$ ratios (~ 0.1−0.4) and ^{192}Os concentrations up to ~ 15,300 pg/g. Such signatures were previously shown to arise from a large transient flux of unradiogenic Os to the oceans during emplacement and weathering of large igneous provinces and intensified hydrothermal activity, which temporarily increased the seawater Os inventory (Fig. 4). In our compilation, this group is represented by the Paleocene-Eocene Thermal Maximum event (ca. 56 Ma) (LIP: the North Atlantic Igneous Province; Dickson et al., 2015), the Cenomanian-Turonian OAE2 (ca. 93.5 Ma) (LIP: the Caribbean-Colombian Igneous Province; Turgeon and Creaser, 2008; Du Vivier et al., 2014, 2015), the early Aptian OAE 1a (ca. 120 Ma) (LIP: the Ontong Java Plateau; Tejada et al., 2009; Bottini et al., 2012), the Sinemurian-Pliensbachian boundary (ca. 190 Ma) (caused by mantle-

derived hydrothermal activity related to the formation of the Hispanic Corridor during Pangaea fragmentation; Porter, 2012; Porter et al., 2013), and the Triassic-Jurassic boundary (200-205 Ma) (LIP: the Central Atlantic Magmatic Province; Cohen et al., 1999; Cohen and Coe, 2002) (Fig. 4, Table A.1 and A.2).

Not all LIPs cause Os enrichment, as recorded by ORM deposited during OAEs. The eruption of the Siberian Traps is commonly associated with the late Permian mass extinction event at the Permian-Triassic boundary (252 Ma; Svensen et al., 2009; Georgiev et al., 2011, 2015; Schoepfer et al., 2013). The ^{192}Os concentrations are not unusually high, and initial $^{187}Os/^{188}Os$ ratios across the extinction horizon are variable, but relatively more radiogenic (0.2 to 0.6) than other LIP events. Because the traps record subaerial (rather than submarine) eruptions, their contribution to seawater is only a small fraction of total continental runoff. More importantly, the magmatic feeders for the Traps transected ORMs and petroleum-bearing evaporites of the Tunguska Basin, releasing gigatons of CO_2 along with significant quantities of methyl chloride and methyl bromide (Svensen et al., 2009). Thus, given the high Os concentrations likely in such organic matter rich sedimentary rocks relative to those of basalts, any contribution of Os to the atmosphere via aerosols or particulate matter was likely highly radiogenic.

Bolide impacts also cause transiently high seawater Os concentrations and unradiogenic seawater $^{187}Os/^{188}Os$, but are not represented in our ORM compilation. Evidence for Os isotopic excursions of very short duration across the Cretaceous-Paleogene boundary have been documented in carbonates and metalliferous pelagic clays

from deep-sea cores (Peucker-Ehrenbrink and Ravizza, 2000), and cliff exposures of chalks straddling the Fish Clay horizon in Denmark (Frei and Frei, 2002; Goswami et al., 2017). These unradiogenic Os inputs during a transient extraterrestrial event are decoupled from atmosphere-ocean O_2 levels and weathering of radiogenic continental crust.

A second group of high ^{192}Os concentrations occurs in Late Ediacaran and Early Cambrian ORM from South China (555-535 Ma) (Mao et al., 2002; Jiang et al., 2007; Lehmann et al., 2007; Kendall et al., 2009b; Pi et al., 2013; Xu et al., 2013; Zhu et al., 2013; Fu et al., 2016) (Fig. 4). These ORM are associated with radiogenic seawater $^{187}Os/^{188}Os$ values of ≥ 0.8 and extremely high ^{192}Os concentrations (up to ~ 26,600 pg/g) that point to significant oxidative mobilization of Os and a strong riverine Os flux. The ca. 535 Ma Niutitang Formation and ca. 555 Ma upper Doushantuo Formation (Member IV) are the main examples in our compilation. However, the controlling factors responsible for these high ^{192}Os concentrations are not well understood. These ORM were deposited at a time of elevated crustal weathering rates associated with Gondwana assembly (Shields-Zhou and Och, 2011). Proximal Os-rich crustal sources and ultraslow sedimentation rates may have contributed to the high ^{192}Os concentrations in the upper Doushantuo Formation (Kendall et al., 2009b; Zhu et al., 2013). Alternatively, other local depositional controls (e.g., water column pH, type of organic matter) may have been important. The origin of extreme metal enrichments in the black shales of the lower Cambrian Niutitang Formation and the origin of a polymetallic Ni-Mo-PGE layer in this

formation have traditionally been controversial (Mao et al., 2002; Jiang et al., 2007; Lehmann et al., 2007; Pi et al., 2013; Xu et al., 2013; Fu et al., 2016). The two most prevalent explanations are a submarine-hydrothermal origin (e.g. Jiang et al., 2007; Pi et al., 2013) and a seawater origin (e.g. Mao et al., 2002; Lehmann et al., 2007; Xu et al., 2013; Fu et al., 2016). A hydrothermal source can account for the formation of the polymetallic sulfide layer, which might also contribute to metal enrichments in the Niutitang Formation. However, high initial $^{187}Os/^{188}Os$ ratios (~ 0.80−0.90) from separate Re-Os isochron regressions of samples from the Ni-Mo-PGE layer and the host, non-mineralized ORM both point to a primarily radiogenic seawater Os source rather than an unradiogenic hydrothermal Os source (Mao et al., 2002; Jiang et al., 2007; Fu et al., 2016). Hence, upwelling of nutrient-rich deep waters into a water-stratified, restricted basin coupled with slow sedimentation rates are thus proposed to be the major controls on the formation of the polymetallic sulfide layer and the metal enrichments in the Niutitang Formation (Mao et al., 2002; Lehmann et al., 2007; Xu et al., 2013; Fu et al., 2016). Such high ^{192}Os concentrations are generally not observed in broadly coeval ORM from India, suggesting that the ^{192}Os enrichments in the Niutitang Formation are a local phenomenon rather than representative of the global ocean.

If these two groups of anomalous ^{192}Os enrichments are excluded, the average ^{192}Os concentration of Ediacaran-Phanerozoic ORM drops to 166 pg/g (1SD = 148, median = 106, n = 25, Table 2). In this case, the mean of 10,000 ^{192}Os bootstrap medians is 112 pg/g with a 95% confidence interval of (72, 168) for the Ediacaran-Phanerozoic

time bin (Table 3). This mean value is not significantly different than that of the pre-Ediacaran Proterozoic time bin (88 pg/g, 95% confidence interval of 35−159). Hence, we conclude that there is no more than a small overall increase in the ^{192}Os concentrations of ORM from the pre-Ediacaran Proterozoic to the Ediacaran-Phanerozoic.

5.3 Relative contributions of radiogenic and unradiogenic Os to the oceans over time and implications for evolution of the sedimentary Os reservoir

Several knowledge gaps hamper our intentions to further constrain the evolution of the seawater Os reservoir. There is no robust evidence that all ORMs in our compilation were deposited without significant basin restrictions (those ORMs with Re < 5 ng/g were excluded from our compilation, as such low concentrations indicate extreme basin restriction; in this case the preserved Os signatures may represent local scenarios rather than regional or global seawater). In addition, no direct relationship has been established between dissolved Os concentrations in the bottom waters and sediment Os concentrations for modern environments. Thus, our ^{192}Os compilation may not capture first-order changes of the seawater Os reservoir between time bins. Furthermore, no correlation is observed between ^{192}Os concentrations and initial ^{187}Os/^{188}Os ratios (Fig. 6); the two time points for the Archean have relatively low ^{192}Os concentrations and unradiogenic ^{187}Os/^{188}Os, but data for all other time points are broadly overlapping. This observation suggests that neither of the two end-member Os seawater sources (radiogenic old continental crust versus unradiogenic mantle, extraterrestrial, and young juvenile,

mafic, and ultramafic crust) represents the major control on the size of the sedimentary Os reservoir for the entirety of the past 3 Gyr. This is a logical expectation given that unradiogenic Os inputs likely dominated the flux of Os to Archean and early Paleoproterozoic seawater, and fluctuations in the relative inputs of radiogenic versus unradiogenic Os to the oceans have occurred since at least 2.5 Ga (the oldest known example of seawater $^{187}Os/^{188}Os$ that is statistically higher than the mantle-extraterrestrial baseline; Kendall et al., 2015a).

We propose that unradiogenic Os from ultramafic seafloor hydrothermal systems and possibly weathering of mafic/ultramafic/juvenile crust were the dominant source of Os in most of the Archean and early Paleoproterozoic ORMs because of the weak riverine flux of Os (due to low atmospheric O_2 levels). The Archean mantle was likely hotter than present day, implying enhanced effusion from ultramafic seafloor hydrothermal systems, production of Os-rich komatiites and olivine-rich basalts in the crust, and perhaps even mafic/ultramafic volcanic landmasses (Shirey and Walker, 1989; Grove and Parman, 2004; Berry et al., 2008; Konhauser et al., 2009; Herzberg et al., 2010; Kamber, 2010; Dhuime et al., 2015; Chen et al., 2016; Sobolev et al., 2016; M. Tang et al., 2016; Ganne and Feng, 2017; Garçon et al., 2017). Komatiites (ultramafic lavas) are enriched in Os and required very high temperature (~ 1600 °C) in the mantle for their formation and eruption (Berry et al., 2008; Konhauser et al., 2009; Herzberg et al., 2010; Sobolev et al., 2016). The greater prevalence of komatiites in the Archean raises the possibility of high unradiogenic Os inputs from ultramafic-hosted hydrothermal systems,

and potentially could explain ^{192}Os enrichments in some Archean ORMs. However, in widely anoxic and Fe(II)-rich Archean oceans, transport distances for Os from seafloor hydrothermal systems may have been short because of the limited solubility of reduced Os species; that is, heterogeneous Archean seawater Os concentrations are possible. Elevated ^{192}Os concentrations and unradiogenic initial $^{187}Os/^{188}Os$ in some Archean deep-sea ORMs may thus suggest relatively close proximity to a seafloor hydrothermal system. By contrast, subaerial chemical weathering of mafic and possibly ultramafic rocks followed by long-distance riverine transport of Os to the oceans is difficult to visualize at Archean atmospheric O_2 levels below ~ 0.001% PAL (based on mass-independent fractionation signatures of sulfur isotopes in Archean sedimentary rocks; Pavlov and Kasting, 2002). At such low O_2 levels, redox reactions involving Os and Fe(II) would probably remove Os from rivers (Kendall et al., 2015a). Alternatively, given the greater preservation opportunities for shelf sediments, Archean ORM with Os enrichments and unradiogenic initial $^{187}Os/^{188}Os$ signatures may have been deposited near weathered Os-rich and less radiogenic mafic/ultramafic terrains.

Changes in the composition of the continental crust, possibly due to declining heat fluxes in Earth's interior and the onset of plate tectonics, likely had an impact on the flux and isotopic composition of Os preserved in ORM. A transition from a relatively more mafic to a more felsic continental crust may have occurred between 3.0 and 2.5 Ga, possibly in association with the advent of plate tectonics (Dhuime et al., 2015; M. Tang et al., 2016). Although felsic crust is more depleted in Os relative to mafic/ultramafic crust,

such a change would have likely increased the Re/Os ratio of the continental crust, ultimately causing the $^{187}Os/^{188}Os$ of the Proterozoic and Phanerozoic continental crust (and thus rivers) to increase at a faster rate. Moreover, elevated atmospheric O_2 contents would stimulate more intense weathering of Os-rich materials in the continental crust (ORM, sulfide minerals) so that more Os could be oxidized and released to rivers. In addition, more oxygenated environments permit a longer transport distance of radiogenic Os in rivers and thus delivery of Os to the oceans. With accumulation of radiogenic crustal-derived Os in the ocean, a more radiogenic Os isotope signature is thus recorded by marine ORM after the GOE.

The first-order increase to more radiogenic seawater $^{187}Os/^{188}Os$ from the pre-Ediacaran Proterozoic to Ediacaran-Phanerozoic demonstrates a larger crustal Os input via rivers due to a more oxygenated atmosphere and weathering of more radiogenic old continental crust. It is extremely difficult, however, to demonstrate which factor is the more important control on the rise in seawater $^{187}Os/^{188}Os$; we simply lack sufficient information to reconstruct the growth of $^{187}Os/^{188}Os$ ratios in the continental crust. Other geological factors including LIPs, climate change (glacial-interglacial interactions), and plate tectonics also influenced seawater $^{187}Os/^{188}Os$ ratios in Proterozoic and Phanerozoic ORM. Lower ^{192}Os concentrations in modern anoxic sediments compared to those in Ediacaran-Phanerozoic ORM suggests that the non-radiogenic Os content of ORM is not solely tied to atmospheric oxygen levels. There must be other factors that control the release and uptake of Os in both modern and ancient systems.

6. CONCLUSIONS

Osmium is a highly compatible trace metal, reaching only pg/g levels in the Earth's continental crust, but has variable $^{187}Os/^{188}Os$ ratios that provide a powerful tracer for the source of Os. The marine geochemical behavior of Os was reviewed in this paper, but several knowledge gaps hamper full understanding of the marine Os cycle, including: 1) poorly constrained Os fluxes from each source; 2) poorly constrained Os fluxes into each sink; 3) mechanisms of Os removal under different redox conditions and into different materials; and 4) factors that influence Os uptake (temperature, pH, type of organic matter, major host of Os). Consequently, large uncertainties remain in the total Os input and output fluxes for the modern ocean, and the overall oceanic mass balance of Os.

Our compilation and statistical analysis of ^{192}Os enrichments from ORM reveals that there was no more than a small overall increase in the ^{192}Os concentrations of ORM from the pre-Ediacaran Proterozoic to the Ediacaran-Phanerozoic. This analysis excluded two groups of anomalously high ^{192}Os concentrations from the Ediacaran-Phanerozoic time bin, which are attributed to unusual local depositional conditions such as proximity to Os-rich crustal sources and/or ultraslow sedimentation rates (for the group with high initial $^{187}Os/^{188}Os$ ratios) and emplacement of large igneous provinces (for the group with low initial $^{187}Os/^{188}Os$ ratios). Very limited Archean ^{192}Os data precludes confident interpretation. Our effort to define the evolution of the seawater Os reservoir over the past

3 Gyr is hampered by the lack of an established relationship between Os concentrations in anoxic sediments and the dissolved Os concentrations of overlying bottom waters in modern anoxic basins and, more generally, an incomplete understanding of Os geochemical behavior and the modern oceanic mass balance of Os.

There is a first-order increase in seawater $^{187}Os/^{188}Os$ ratios (as inferred from the initial $^{187}Os/^{188}Os$ ratios calculated from Re-Os isochron regressions) from the Archean to Phanerozoic. Most Archean and early Paleoproterozoic ORM have initial $^{187}Os/^{188}Os$ ratios that are indistinguishable from the mantle-extraterrestrial baseline, indicating that the major Os source to the oceans at that time was unradiogenic Os from seafloor hydrothermal systems and weathering of less radiogenic mafic/ultramafic/juvenile crust. Subsequently, the development of a radiogenic riverine Os flux associated with increased atmosphere-ocean oxygenation and weathering of more radiogenic continental crust was responsible for the overall higher initial $^{187}Os/^{188}Os$ ratios in Ediacaran-Phanerozoic ORM. Superimposed on this first-order trend in seawater $^{187}Os/^{188}Os$ were shorter-term fluctuations related to other geological factors, including the emplacement of LIPs, climate change, and plate tectonic reorganizations.

Acknowledgements

This study was supported by an NSERC Discovery Grant to BK (RGPIN-435930). Alex Sheen is thanked for assistance with compilation of Re data. We are grateful to three anonymous reviewers, Alan Rooney, and editor Laurie Reisberg for constructive

comments that significantly improved this manuscript. We acknowledge the dedicated efforts of many sedimentary Os geochemistry groups whose hard work helped make it possible to produce an Os compilation for organic-rich mudrocks.

REFERENCES

Aitken J. D. (1991) Two Late Proterozoic glaciations, Mackenzie Mountains, northwestern Canada. *Geology* **19**, 445-448.

Algeo T. J. and Lyons T. W. (2006) Mo-total organic carbon covariation in modern anoxic marine environments: Implications for analysis of paleoredox and paleohydrographic conditions. *Paleoceanography* **21**, PA1016.

Anbar A. D., Duan Y., Lyons T. W., Arnold G. L., Kendall B., Creaser R. A., Kaufman A. J., Gordon G. W., Scott C., Garvin J. and Buick R. (2007) A Whiff of Oxygen Before the Great Oxidation Event? *Science* **317**, 1903-1906.

Baioumy H. M., Eglinton L. B. and Peucker-Ehrenbrink B. (2011) Rhenium–osmium isotope and platinum group element systematics of marine vs. non-marine organic-rich sediments and coals from Egypt. *Chem. Geol.* **285**, 70-81.

Barnes C. E. and Cochran J. K. (1990) Uranium removal in oceanic sediments and the oceanic U balance. *Earth Planet. Sci. Lett.* **97**, 94-101.

Bender M. L., Ku T. L. and Broecker W. S. (1970) Accumulation rates of manganese in pelagic sediments and nodules. *Earth Planet. Sci. Lett.* **8**, 143-148.

Berner E. K. and Berner R. A. (1987) The global Water Cycle, Prentice-Hall, Englexood Cliffs, New Jersey, 397 pp.

Berry A. J., Danyushevsky L. V., O'Neill H. S. C., Newville M. and Sutton S. R. (2008) Oxidation state of iron in komatiitic melt inclusions indicates hot Archean mantle. *Nature* **455**, 960-963.

Bottini C., Cohen A. S., Erba E., Jenkyns H. C. and Coe A. L. (2012) Osmium-isotope evidence for volcanism, weathering, and ocean mixing during the early Aptian OAE 1a. *Geology* **40**, 583-586.

Burton K. W., Bourdon B., Birck J. L., Allègre C. J. and Hein J. R. (1999) Osmium isotope variations in the oceans recorded by Fe-Mn crusts. *Earth Planet. Sci. Lett.* **171**, 185-197.

Cave R. R., Ravizza G. E., German C. R., Thomson J. and Nesbitt R. W. (2003) Deposition of osmium and other platinum-group elements beneath the ultramafic-hosted Rainbow hydrothermal plume. *Earth Planet. Sci. Lett.* **210**, 65-79.

Chen C., Sedwick P. N. and Sharma M. (2009) Anthropogenic osmium in rain and snow reveals global-scale atmospheric contamination. *Proc. Natl. Acad. Sci. U.S.A.* **106**, 7724-7728.

Chen C. and Sharma M. (2009) High precision and high sensitivity measurements of osmium in seawater. *Anal. Chem.* **81**, 5400-5406.

Chen C., Sharma M. and Bostick B. C. (2006) Lithologic controls on osmium isotopes in the Rio Orinoco. *Earth Planet. Sci. Lett.* **252**, 138-151

Chen K., Walker R. J., Rudnick R. L., Gao S., Gaschnig R. M., Puchtel I. S., Tang M. and Hu Z.-C. (2016) Platinum-group element abundances and Re-Os isotopic systematics of the upper continental crust through time: Evidence from glacial diamictites. *Geochim. Cosmochim. Acta* **191**, 1-16.

Cohen A. S., Coe A. L., Bartlett J. M. and Hawkesworth C. J. (1999) Precise Re-Os ages of organic-rich mudrocks and the Os isotope composition of Jurassic seawater. *Earth Planet. Sci. Lett.* **167**, 159-173.

Cohen A. S. and Coe A. L. (2002) New geochemical evidence for the onset of volcanism in the Central Atlantic magmatic province and environmental change at the Triassic-Jurassic boundary. *Geology* **30**, 267-270.

Crocket J. H. (1979) Platinum-group elements in mafic and ultramafic rocks: A survey. *Can. Mineral.* **17**, 391-402.

Crusius J., Calvert S., Pedersen T. and Sage D. (1996) Rhenium and molybdenum enrichments in sediments as indicators of oxic, suboxic and sulfidic conditions of deposition. *Earth Planet. Sci. Lett.* **145**, 65-78.

Dalai T. K. and Ravizza G. (2006) Evaluation of osmium isotopes and iridium as paleoflux tracers in pelagic carbonates. *Geochim. Cosmochim. Acta* **70**, 3928-3942.

Dalai T. K., Suzuki K., Minagawa M. and Nozaki Y. (2005) Variations in seawater osmium isotope composition since the last glacial maximum: A case study from the Japan Sea. *Chem. Geol.* **220**, 303-314.

Dean W. E. (2006) The geochemical record of the last 17,000 years in the Guaymas Basin, Gulf of California. *Chem. Geol.* **232**, 87-98.

Dhuime B., Wuestefeld A. and Hawkesworth C. J. (2015) Emergence of modern continental crust about 3 billion years ago. *Nat. Geosci.* **8**, 552-555.

Dickson A. J., Cohen A. S., Coe A. L., Davies M., Shcherbinina E. A. and Gavrilov Y. O. (2015) Evidence for weathering and volcanism during the PETM from Arctic Ocean and Peri-Tethys osmium isotope records. *Palaeogeogr. Palaeoclimatol. Palaeoecol.* **438**, 300-307.

Dubin A. and Peucker-Ehrenbrink B. (2015) The importance of organic-rich shales to the geochemical cycles of rhenium and osmium. *Chem. Geol.* **403**, 111-120.

Dunk R. M., Mills R. A. and Jenkins W. J. (2002) A reevaluation of the oceanic uranium budget for the Holocene. *Chem. Geol.* **190**, 45-67.

Du Vivier A. D. C., Selby D., Condon D. J., Takashima R. and Nishi H. (2015) Pacific $^{187}Os/^{188}Os$ isotope chemistry and U–Pb geochronology: Synchroneity of global Os isotope change across OAE 2. *Earth Planet. Sci. Lett.* **428**, 204-216.

Du Vivier A. D. C., Selby D., Sageman B. B., Jarvis I., Gröcke D. R. and Voigt S. (2014) Marine $^{187}Os/^{188}Os$ isotope stratigraphy reveals the interaction of volcanism and ocean circulation during Oceanic Anoxic Event 2. *Earth Planet. Sci. Lett.* **389**, 23-33.

Efron B. (1979) Bootstrap methods: another look at the jackknife. *Ann. Stat.* **7**, 1-26.

Erickson B. E. and Helz G. R. (2000) Molybdenum(VI) speciation in sulfidic waters: Stability and lability of thiomolybdates. *Geochim. Cosmochim. Acta* **64**, 1149-1158.

Esser B. K. and Turekian K. K. (1993) The osmium isotopic composition of the continental crust. *Geochim. Cosmochim. Acta* **57**, 3093-3104.

Frei R. and Frei K. M. (2002) A multi-isotopic and trace element investigation of the Creaceous-Tertiary boundary layer at Stevns Klint, Denmark – inferences for the

origin and nature of siderophile and lithophile element geochemical anomalies. *Earth Planet. Sci. Lett.* **203**, 691-708.

Fu Y., Dong L., Li C., Qu W., Pei H., Qiao W. and Shen B. (2016) New Re-Os isotopic constrains on the formation of the metalliferous deposits of the Lower Cambrian Niutitang formation. *J. Earth Sci.* **27**, 271-281.

Ganne J. and Feng X. (2017) Primary magmas and mantle temperatures through time. *Geochem. Geophys. Geosyst.* **18**, 872-888.

Gannoun A., Burton K. W., Vigier N., Gislason S. R., Rogers N., Mokadem F. and Sigfússon B. (2006) The influence of weathering process on riverine osmium isotopes in a basaltic terrain. *Earth Planet. Sci. Lett.* **243**, 732-748.

Garçon M., Carlson R. W., Shirey S. B., Arndt N. T., Horan M. F. and Mock T. D. (2017) Erosion of Archean continents: The Sm-Nd and Lu-Hf isotopic record of Barberton sedimentary rocks. *Geochim. Cosmochim. Acta* **206**, 216-235.

Georg R. B., West A. J., Vance D., Newman K. and Halliday A. N. (2013) Is the marine osmium isotope record a probe for CO_2 release from sedimentary rocks? *Earth Planet. Sci. Lett.* **367**, 28-38.

Georgiev S., Stein H. J., Hannah J. L., Bingen B., Weiss H. M. and Piasecki S. (2011) Hot acidic Late Permian seas stifle life in record time. *Earth Planet. Sci. Lett.* **310**, 389-400.

Georgiev S. V., Stein H. J., Hannah J. L., Henderson C. M. and Algeo T. J. (2015) Enhanced recycling of organic matter and Os-isotopic evidence for multiple

magmatic or meteoritic inputs to the Late Permian Panthalassic Ocean, Opal Creek, Canada. *Geochim. Cosmochim. Acta* **150**, 192-210.

Golden J., McMillan M., Downs R. T., Hystad G., Goldstein I., Stein H. J., Zimmerman A., Sverjensky D. A., Armstrong J. T. and Hazen R. M. (2013) Rhenium variations in molybdenite (MoS_2): Evidence for progressive subsurface oxidation. *Earth Planet. Sci. Lett.* **366**, 1-5.

Goswami V., Stein H. J. and Hannah J. L. (2017) Variation in $^{187}Os/^{188}Os$ across K-T boundary at Stevns Klint, Denmark. *Goldschmidt Conf. Abs.* no. 2538.

Grove T. L. and Parman S. W. (2004) Thermal evolution of the Earth as recorded by komatiites. *Earth Planet. Sci. Lett.* **219**, 173-187.

Hannah J. L., Bekker A., Stein H. J., Markey R. J. and Holland H. D. (2004) Primitive Os and 2316 Ma age for marine shale: implications for Paleoproterozoic glacial events and the rise of atmospheric oxygen. *Earth Planet. Sci. Lett.* **225**, 43-52.

Hannah J. L. and Stein H. J. (2012) Re-Os Geochemistry. In *Reading the Archive of Earth's Oxygenation*, Volume 3: Global Events and the Fennoscandian Arctic Russia – Drilling Early Earth Project (eds. V. A. Melezhik, L. R. Kump, A. E. Fallick, H. Strauss, E. J. Hanski, A. R. Prave and A. Lepland). Springer-Verlag, Berlin, Heidelberg. pp. 1506-1514.

Hattori Y., Suzuki K., Honda M. and Shimizu H. (2003) Re–Os isotope systematics of the Taklimakan Desert sands, moraines and river sediments around the Taklimakan Desert, and of Tibetan soils. *Geochim. Cosmochim. Acta* **67**, 1203-1213.

Herzberg C., Condie K. and Korenaga J. (2010) Thermal history of the Earth and its petrological expression. *Earth Planet. Sci. Lett.* **292**, 79-88.

Huh Y., Birck J. L. and Allègre C. J. (2004) Osmium isotope geochemistry in the Mackenzie River basin. *Earth Planet. Sci. Lett.* **222**, 115-129.

Jiang S., Yang J., Ling H., Chen Y., Feng H., Zhao K. and Ni P. (2007) Extreme enrichment of polymetallic Ni–Mo–PGE–Au in Lower Cambrian black shales of South China: An Os isotope and PGE geochemical investigation. *Palaeogeogr. Palaeoclimatol. Palaeoecol.* **254**, 217-228.

Kamber B. S. (2010) Archean mafic–ultramafic volcanic landmasses and their effect on ocean–atmosphere chemistry. *Chem. Geol.* **274**, 19-28.

Kendall B., Creaser R. A., Calver C. R., Raub T. D. and Evans D. A. D. (2009a) Correlation of Sturtian diamictite successions in southern Australia and northwestern Tasmania by Re-Os black shale geochronology and the ambiguity of "Sturtian" - type diamictite-cap carbonate pairs as chronostratigraphic marker horizons. *Precambrian Res.* **172**, 301-310.

Kendall B., Creaser R. A. and Selby D. (2006) Re-Os geochronology of postglacial black shales in Australia: Constraints on the timing of “Sturtian” glaciation. *Geology* **34**, 729-732.

Kendall B., Creaser R. A. and Selby D. (2009b) ^{187}Re-^{187}Os geochronology of Precambrian organic-rich sedimentary rocks. *Geol. Soc. London Spec. Publ.* **326**, 85-107.

Kendall B., Creaser R. A., Reinhard C. T., Lyons T. W. and Anbar A. D. (2015a) Transient episodes of mild environmental oxygenation and oxidative continental weathering during the late Archean. *Sci. Adv.* **1**, e1500777.

Kendall B., Komiya T., Lyons T. W., Bates S. M., Gordon G. W., Romaniello S. J., Jiang G., Creaser R. A., Xiao S., McFadden K., Sawaki Y., Tahata M., Shu D., Han J., Li Y., Chu X. and Anbar A. D. (2015b) Uranium and molybdenum isotope evidence for an episode of widespread ocean oxygenation during the late Ediacaran Period. *Geochim. Cosmochim. Acta* **156**, 173-193.

Koide M., Goldberg E. D., Niemeyer S., Gerlach D., Hodge V., Bertine K. K. and Padova A. (1991) Osmium in marine sediments. *Geochim. Cosmochim. Acta* **55**, 1641-1648.

Konhauser K. O., Pecoits E., Lalonde S. V., Papineau D., Nisbet E. G., Barley M. E., Arndt N. T., Zahnle K. and Kamber B. S. (2009) Oceanic nickel depletion and a methanogen famine before the Great Oxidation Event. *Nature* **458**, 750-753.

Konhauser K. O., Robbins L. J., Pecoits E., Peacock C. L., Kappler A. and Lalonde S. V. (2015) The Archean nickel famine revisited. *Astrobiology* **15**, 804-815.

Krähenbühl U., Geissbühler M., Bühler F., Eberhardt P. and Finnegan D. L. (1992) Osmium isotopes in the aerosols of the mantle volcano Mauna Loa. *Earth Planet. Sci. Lett.* **110**, 95-98.

Ku T. L., Knauss K. G. and Mathieu G. G. (1977) Uranium in open ocean: concentration and isotopic composition*. *Deep Sea Res.* **24**, 1005-1017.

Large R. R., Halpin J. A., Danyushevsky L. V., Maslennikov V. V., Bull S. W., Long J. A., Gregory D. D., Lounejeva E., Lyons T. W., Sack P. J., McGoldrick P. J. and Calver C. R. (2014) Trace element content of sedimentary pyrite as a new proxy for deep-time ocean-atmosphere evolution. *Earth Planet. Sci. Lett.* **389**, 209-220.

Large R. R., Halpin J. A., Lounejeva E., Danyushevsky L. V., Maslennikov V. V., Gregory D., Sack P. J., Haines P. W., Long J. A., Makoundi C. and Stepanov A. S. (2015) Cycles of nutrient trace elements in the Phanerozoic ocean. *Gondwana Res.* **28**, 1282-1293.

Lehmann B., Nägler T. F., Holland H. D., Wille M., Mao J., Pan J., Ma D. and Dulski P. (2007) Highly metalliferous carbonaceous shale and Early Cambrian seawater. *Geology* **35**, 403-406.

Levasseur S., Birck J. L. and Allègre C. J. (1998) Direct measurement of femtomoles of osmium and the $^{187}Os/^{186}Os$ ratio in seawater. *Science* **282**, 272-274.

Levasseur S. Birck J. L. and Allègre C. J. (1999) The osmium riverine flux and the oceanic mass balance of osmium. *Earth Planet. Sci. Lett.* **174**, 7-23.

Ludwig K. (2011) Isoplot/Ex Version 4: *A Geochronological Toolkit for Microsoft Excel*. Geochronology Center, Berkeley.

Luke J. M. and Allègre C. J. (1983) ^{187}Re-^{187}Os systematics in meteorites and cosmochemical consequences. *Nature* **302**, 130-132.

Lyons T. W., Reinhard C. T. and Planavsky N. J. (2014) The rise of oxygen in Earth's early ocean and atmosphere. *Nature* **506**, 307-315.

Lyons T. W. and Severmann, S. (2006) A critical look at iron paleoredox proxies: New insights from modern euxinic marine basins. *Geochim. Cosmochim. Acta* **70**, 5698-5722.

Martin C. E., Peucker-Ehrenbrink B., Brunskill G. J. and Szymczak R. (2000) Sources and sinks of unradiogenic osmium runoff from Papua New Guinea. *Earth Planet. Sci. Lett.* **183**, 261-274

Mao J., Lehmann B., Du A., Zhang G., Ma D., Wang Y., Zeng M. and Kerrich R. (2002) Re-Os dating of polymetallic Ni-Mo-PGE-Au mineralization in lower Cambrian black shales of south China and its geologic significance. *Econ. Geol.* **97**, 1051-1061.

McArthur J. M., Algeo T. J., van de Schootbrugge B., Li Q. and Howarth R. J. (2008) Basinal restriction, black shales, and the Early Toarcian (Jurassic) Oceanic Anoxic Event. *Paleoceanography* **23**, PA4217.

McDaniel D. K., Walker R. J., Hemming S. R., Horan M. F., Becker H. and Grauch R. I. (2004) Sources of osmium to the modern oceans: new evidence from the ^{190}Pt-^{186}Os system. *Geochim. Cosmochim. Acta* **68**, 1243-1252.

McLennan S. M. (2001) Relationships between the trace element composition of sedimentary rocks and upper continental crust. *Geochem. Geophys. Geosyst.* **2**, 2000GC000109.

Miller C. A., Peucker-Ehrenbrink B., Walker B. D. and Marcantonio F. (2011) Re-assessing the surface cycling of molybdenum and rhenium. *Geochim. Cosmochim. Acta* **75**, 7146-7179.

Morelli R. M., Creaser R. A., Selby D., Kelly K. D., Leach D. L. and King A. R. (2004) Re-Os sulfide geochronology of the Red Dog sediment-hosted Zn-Pb-Ag deposit, Brooks Range, Alaska. *Econ. Geol.* **99**, 1569-1576.

Morford J. L. and Emerson S. (1999) The geochemistry of redox sensitive trace metals in sediments. *Geochim. Cosmochim. Acta* **63**, 1735-1750.

Morford J. L., Emerson S. R., Breckel E. J. and Kim S. H. (2005) Diagenesis of oxyanions (V, U, Re, and Mo) in pore waters and sediments from a continental margin. *Geochim. Cosmochim. Acta* **69**, 5021-5032.

Morford J. L., Martin W. R. and Carney C. M. (2012) Rhenium geochemical cycling: Insights from continental margins. *Chem. Geol.* **324-325**, 73-86.

Oxburgh R. (2001) Residence time of osmium in the oceans. *Geochem. Geophys. Geosyst.* **2**, 2000GC000104.

Oxburgh R., Pierson-Wickmann A., Reisberg L. and Hemming S. (2007) Climate-correlated variations in seawater $^{187}Os/^{188}Os$ over the past 200,000 yr: Evidence from the Cariaco Basin, Venezuela. *Earth Planet. Sci. Lett.* **263**, 246-258.

Paquay F. S. and Ravizza G. (2012) Heterogeneous seawater $^{187}Os/^{188}Os$ during the Late Pleistocene glaciations. *Earth Planet. Sci. Lett.* **349-350**, 126-138.

Partin C. A., Bekker A., Planavsky N. J., Scott C. T., Gill B. C., Li C., Podkovyrov V., Maslov A., Konhauser K. O., Lalonde S. V., Love G. D., Poulton S. W. and Lyons T. W. (2013a) Large-scale fluctuations in Precambrian atmospheric and oceanic

oxygen levels from the record of U in shales. *Earth Planet. Sci. Lett.* **369-370**, 284-293.

Partin C. A., Lalonde S. V., Planavsky N. J., Bekker A., Rouxel O. J., Lyons T. W. and Konhauser K. O. (2013b) Uranium in iron formations and the rise of atmospheric oxygen. *Chem. Geol.* **362**, 82-90.

Paul M., Reisberg L., Vigier N., Zheng Y., Ahmed K. M., Charlet L. and Huq M. R. (2010) Dissolved osmium in Bengal plain groundwater: Implications for the marine Os budget. *Geochim. Cosmochim. Acta* **74**, 3432-3448.

Pavlov A. A. and Kasting J. F. (2002) Mass-Independent Fractionation of Sulfur Isotopes in Archean Sediments: Strong Evidence for an Anoxic Archean Atmosphere. *Astrobiology* **2**, 27-41.

Peucker-Ehrenbrink, B. (2002). Comment on "Residence time of osmium in the oceans" by Rachel Oxburgh. *Geochem. Geophys. Geosyst.* **3**, 1-4.

Peucker-Ehrenbrink B. and Jahn B. (2001) Rhenium-osmium isotope systematics and platinum group element concentrations: Loess and the upper continental crust. *Geochem. Geophys. Geosyst.* **2**, 2001GC000172.

Peucker-Ehrenbrink B. and Ravizza G. (2000) The marine osmium isotope record. *Terra Nova* **12**, 205-219.

Peucker-Ehrenbrink B., Ravizza G. and Hofmann A. W. (1995) The marine $^{187}Os/^{186}Os$ record of the past 80 million years. *Earth Planet. Sci. Lett.* **130**, 155-167.

Pi D., Liu C., Shields-Zhou G. A. and Jiang S. (2013) Trace and rare earth element geochemistry of black shale and kerogen in the early Cambrian Niutitang Formation in Guizhou province, South China: Constraints for redox environments and origin of metal enrichments. *Precambrian Res.* **225**, 218-229.

Poirier A. (2006) Re–Os and Pb isotope systematics in reduced fjord sediments from Saanich Inlet (Western Canada). *Earth Planet. Sci. Lett.* **249**, 119-131.

Porter S. J. (2012) Nickel and osmium isotope and trace element geochemistry of organic-rich sedimentary rocks: The first investigation of Ni isotope systematics in marine sediments. Ph. D. thesis, Durham Univ.

Porter S. J., Selby D., Suzuki K. and Gröcke D. (2013) Opening of a trans-Pangaean marine corridor during the Early Jurassic: Insights from osmium isotopes across the Sinemurian–Pliensbachian GSSP, Robin Hood's Bay, UK. *Palaeogeogr. Palaeoclimatol. Palaeoecol.* **375**, 50-58.

Poulton S. W. and Canfield D. E. (2005) Development of a sequential extraction procedure for iron: implications for iron partitioning in continentally derived particulates. *Chem. Geol.* **214**, 209-221.

Poulton S. W. and Canfield D. E. (2011) Ferruginous Conditions: A Dominant Feature of the Ocean through Earth's History. *Elements* **7**, 107-112.

Poulton S. W. and Raiswell R. (2002) The low-temperature geochemical cycle of iron: From continental fluxes to marine sediment deposition. *Am. J. Sci.* **302**, 774-805.

Raiswell R., Berner R. A. and Anderson T. F. (1988) Degree of pyritization of iron as a paleoenvironmental indicator of bottome-water oxygenation. *J. Sediment. Petrol.* **58**, 812-819.

Raiswell R. and Canfield D. E. (1998) Sources of iron for pyrite formation in marine sediments. *Am. J. Sci.* **298**, 219-245.

Raiswell R., Canfield D. E. and Berner R. A. (1994) A comparison of iron extraction methods for the determination of degree of pyritisation and the recognition of iron-limited pyrite formation. *Chem. Geol.* **111**, 101-111.

Rauch S., Peucker-Ehrenbrink B., Kylander M. E., Weiss D. J., Martinez-Cortizas A., Heslop D., Olid C., Mighall T. M. and Hemond H. F. (2010) Anthropogenic forcings on the surficial osmium cycle. *Environ. Sci. Technol.* **44**, 881-887.

Ravizza G. (1993) Variations of the $^{187}Os/^{186}Os$ ratio of seawater over the past 28 million years as inferred from metalliferous carbonates. *Earth Planet. Sci. Lett.* **118**, 335-348.

Ravizza G., Martin C. E., German C. R. and Thompson G. (1996) Os isotopes as tracers in seafloor hydrothermal systems: metalliferous deposits from the TAG hydrothermal area, 26°N Mid-Atlantic Ridge. *Earth Planet. Sci. Lett.* **138**, 105-119.

Ravizza G., Norris R. N., Blusztajn J. and Aubry M. P. (2001) An osmium isotope excursion associated with the Late Paleocene thermal maximum: Evidence of intensified chemical weathering. *Paleoceanography*, **16**, 155-163.

Ravizza G. and Turekian K. K. (1992) The osmium isotopic composition of organic-rich marine sediments. *Earth Planet. Sci. Lett.* **110**, 1-6.

Ravizza G., Turekian K. K. and Hay B. J. (1991) The geochemistry of rhenium and osmium in recent sediments from the Black Sea. *Geochim. Cosmochim. Acta* **55**, 3741-3752.

Reinhard C. T., Planavsky N. J., Robbins L. J., Partin C. A., Gill B. C., Lalonde S. V., Bekker A., Konhauser K. O. and Lyons T. W. (2013) Proterozoic ocean redox and biogeochemical stasis. *Proc. Natl. Acad. Sci. U.S.A.* **110**, 5357-5362.

Ripley E. M., Park Y., Lambert D. D. and Frick L. R. (2001) Re-Os isotopic composition and PGE contents of Proterozoic carbonaceous argillites, Virginia, Virginia Formation, Northeastern Minnesota. *Org. Geochem.* **32**, 857-866.

Robbins L. J., Lalonde S. V., Saito M. A., Planavsky N. J., Mloszewska A. M., Pecoits E., Scott C., Dupont C. L., Kapple A. and Konhauser K. O. (2013) Authigenic iron oxide proxies for marine zinc over geological time and implications for eukaryotic metallome evolution. *Geobiology* **11**, 295-306.

Robbins L. J., Lalonde S. V., Planavsky N. J., Partin C. A., Reinhard C. T., Kendall B., Scott C., Hardisty D. S., Gill B. C., Alessi D. S., Dupont C. L., Saito M. A., Poulton S. W., Bekker A., Lyons T. W. and Konhauser K. O. (2016) Trace elements at the intersection of marine biological and geochemical evolution. *Earth-Sci. Rev.* **163**, 323-348.

Rooney A. D., Selby D., Houzay J. and Renne P. R. (2010) Re–Os geochronology of a Mesoproterozoic sedimentary succession, Taoudeni basin, Mauritania: Implications for basin-wide correlations and Re–Os organic-rich sediments systematics. *Earth Planet. Sci. Lett.* **289**, 486-496.

Rooney A. D., Selby D., Lloyd J. M., Roberts D. H., Lückge A., Sageman B. B. and Prouty N. G. (2016) Tracking millennial-scale Holocene glacial advance and retreat using osmium isotopes: Insights from the Greenland ice sheet. *Quat. Sci. Rev.* **138**, 49-61.

Rooney A. D., Strauss J. V., Brandon A. D. and Macdonald F. A. (2015) A Cryogenian chronology: Two long-lasting synchronous Neoproterozoic glaciations. *Geology* **43**, 459-462.

Saal A. E., Takazawa E., Frey F. A., Shimizu N. and Hart S. R. (2001) Re-Os isotopes in the Horoman peridotite: Evidence for refertilization? *J. Petrol.* **42**, 25-37.

Sahoo S. K., Planavsky N. J., Kendall B., Wang X., Shi X., Scott C., Anbar A. D., Lyons T. W. and Jiang G. (2012) Ocean oxygenation in the wake of the Marinoan glaciation. *Nature* **489**, 546-549.

Schoepfer S. D., Henderson C. M., Garrison G. H., Foriel J., Ward P. D., Selby D., Hower J. C., Algeo T. J. and Shen Y. (2013) Termination of a continent-margin upwelling system at the Permian–Triassic boundary (Opal Creek, Alberta, Canada). *Glob. Planet. Chang.* **105**, 21-35.

Scott C. and Lyons T. W. (2012) Contrasting molybdenum cycling and isotopic properties in euxinic versus non-euxinic sediments and sedimentary rocks: Refining the paleoproxies. *Chem. Geol.* **324-325**, 19-27.

Scott C., Lyons T. W., Bekker A., Shen Y., Poulton S. W., Chu X. and Anbar A. D. (2008) Tracing the stepwise oxygenation of the Proterozoic ocean. *Nature* **452**, 456-459.

Scott C., Planavsky N. J., Dupont C. L., Kendall B., Gill B. C., Robbins L. J., Husband K. F., Arnold G. L., Wing B. A., Poulton S. W., Bekker A., Anbar A. D., Konhauser K. O. and Lyons T. W. (2013) Bioavailability of zinc in marine systems through time. *Nat. Geosci.* **6**, 125-128.

Selby D. (2007) Direct Rhenium-Osmium age of the Oxfordian-Kimmeridgian boundary, Staffin bay, Isle of Skye, U.K., and the Late Jurassic time scale. *Norw. J. Geol.* **87**, 291-299.

Selby D. and Creaser R. A. (2003) Re–Os geochronology of organic rich sediments: an evaluation of organic matter analysis methods. *Chem. Geol.* **200**, 225-240.

Selby D. and Creaser R. A. (2005) Direct radiometric dating of the Devonian-Mississippian time-scale boundary using the Re-Os black shale geochronometer. *Geology* **33**, 545-548.

Sharma M. (2012) Applications of Osmium and Iridium as Biogeochemical Tracers in the Environment. In *Handbook of Environmental Isotope Geochemistry: Vol I* (eds. M. Baskaran). Springer, Berlin Heidelberg. pp. 205-227.

Sharma M., Balakrishna K., Hofmann A. W. and Shankar R. (2007a) The transport of Osmium and Strontium isotopes through a tropical estuary. *Geochim. Cosmochim. Acta* **71**, 4856-4867.

Sharma M., Papanastassiou D. A. and Wasserburg G. J. (1997) The concentration and isotopic composition of osmium in the oceans. *Geochim. Cosmochim. Acta* **61**, 3287-3299.

Sharma M., Rosenberg E. J. and Butterfield D. A. (2007b) Search for the proverbial mantle osmium sources to the oceans: Hydrothermal alteration of mid-ocean ridge basalt. *Geochim. Cosmochim. Acta* **71**, 4655-4667.

Sharma M., Wasserburg G. J., Hofmann A. W. and Butterfield D. A. (2000) Osmium isotopes in hydrothermal fluids from the Juan de Fuca Ridge. *Earth Planet. Sci. Lett.* **179**, 139-152.

Shields-Zhou G. and Och L. (2011) The case for a Neoproterozoic Oxygenation Event: Geochemical evidence and biological consequences. *GSA Today* **21**, 4-11.

Shirey S. B. and Walker R. J. (1998) The Re-Os isotope system in cosmochemistry and high-temperature geochemistry. *Annu. Rev. Earth Planet. Sci.* **26**, 423-500.

Sims K. W. W., Peucker-Ehrenbrink B., Mather T., Pyle D. M., Martin R., Gauthier P. -J. and Aiuppa A. (2005) Sniffing for clues to the dinosaurs' demise: Measurement of osmium isotope compositions and platinum group element abundances in volcanic emissions. *Fall AGU EOS Trans.* **86**, V21E-0669.

Sobolev A. V., Asafov E. V., Gurenko A. A., Arndt N. T., Batanova V. G., Portnyagin M. V., Garbe-Schönberg D. and Krasheninnikov S. P. (2016) Komatiites reveal a hydrous Archaean deep-mantle reservoir. *Nature* **531**, 628-632.

Sperling E. A., Rooney A. D., Hays L., Sergeev V. N., Vorob'eva N. G., Sergeeva N. D., Selby D., Johnston D. T. and Knoll A. H. (2014) Redox heterogeneity of subsurface waters in the Mesoproterozoic ocean. *Geobiology* **12**, 373-386.

Stein H. J. and Hannah J. L. (2014) The emerging potential of Re-Os isotope geochemistry for source rocks and maturation-migration histories. *IPTC,* 17693.

Stein H. J., Markey R. J., Morgan J. W., Hannah J. L. and Scherstén A. (2001) The remarkable Re-Os chronometer in molybdenite: how and why it works. *Terra Nova* **13**, 479-486.

Stüeken E. E., Buick R., Bekker A., Catling D., Foriel J., Guy B. M., Kah L. C., Machel H. G., Montañez I. P. and Poulton S. W. (2015) The evolution of the global selenium cycle: Secular trends in Se isotopes and abundances. *Geochim. Cosmochim. Acta* **162**, 109-125.

Svensen H., Planke S., Polozov A. G., Schmidbauer N., Corfu F., Podladchikov Y. Y. and Jamtveit B. (2009) Siberian gas venting and the end-Permian environmental crisis. *Earth Planet. Sci. Lett.* **277**, 490-500.

Swanner E. D., Planavsky N. J., Lalonde S. V., Robbins L. J., Bekker A., Rouxel O. J., Saito M. A., Kappler A., Mojzsis S. J. and Konhauser K. O. (2014) Cobalt and marine redox evolution. *Earth Planet. Sci. Lett.* **390**, 253-263.

Tang D., Shi X., Wang X. and Jiang G. (2016) Extremely low oxygen concentration in mid-Proterozoic shallow seawaters. *Precambrian Res.* **276**, 145-157.

Tang M., Chen K. and Rudnick R. L. (2016) Archean upper crust transition from mafic to felsic marks the onset of plate tectonics. *Science* **351**, 372-375.

Tejada M. L. G., Suzuki K., Kuroda J., Coccioni R., Mahoney J. J., Ohkouchi N., Sakamoto T. and Tatsumi Y. (2009) Ontong Java Plateau eruption as a trigger for the early Aptian oceanic anoxic event. *Geology* **37**, 855-858.

Turekian K. K., Sharma M. and Gordon G. W. (2007) The behavior of natural and anthropogenic osmium in the Hudson River–Long Island Sound estuarine system. *Geochim. Cosmochim. Acta* **71**, 4135-4140.

Turgeon S. C. and Creaser R. A. (2008) Cretaceous oceanic anoxic event 2 triggered by a massive magmatic episode. *Nature* **454**, 323-326.

Turgeon S. C., Creaser R. A. and Algeo T. J. (2007) Re–Os depositional ages and seawater Os estimates for the Frasnian–Famennian boundary: Implications for weathering rates, land plant evolution, and extinction mechanisms. *Earth Planet. Sci. Lett.* **261**, 649-661.

van Acken D., Thomson D., Rainbird R. H. and Creaser R. A. (2013) Constraining the depositional history of the Neoproterozoic Shaler Supergroup, Amundsen Basin, NW Canada: Rhenium-osmium dating of black shales from the Wynniatt and Boot Inlet Formations. *Precambrian Res.* **236**, 124-131.

Veeh H. H. (1968) Deposition of uranium from the ocean. *Earth Planet. Sci. Lett.* **3**, 145–150.

Walker R. J., Horan M. F., Morgan J. W., Becker H., Grossman J. N. and Rubin A. E. (2002) Comparative ^{187}Re-^{187}Os systematics of chondrites: Implications regarding early solar system processes. *Geochim. Cosmochim. Acta* **66**, 4187-4201.

Woodhouse O. B., Ravizza G., Falkner K. K., Statham P. J. and Peucker-Ehrenbrink B. (1999) Osmium in seawater: vertical profiles of concentration and isotopic composition in the eastern Pacific Ocean. *Earth Planet. Sci. Lett.* **173**, 223-233

Xu G., Hannah J. L., Stein H. J., Bingen B., Yang G., Zimmerman A., Weitschat W., Mørk A. and Weiss H. M. (2009) Re–Os geochronology of Arctic black shales to evaluate the Anisian–Ladinian boundary and global faunal correlations. *Earth Planet. Sci. Lett.* **288**, 581-587.

Xu G., Hannah J. L., Stein H. J., Mørk A., Vigran J. O., Bingen B., Schutt D. L. and Lundschien B. A. (2014) Cause of Upper Triassic climate crisis revealed by Re–Os geochemistry of Boreal black shales. *Palaeogeogr. Palaeoclimatol. Palaeoecol.* **395**, 222-232.

Xu L., Lehmann B. and Mao J. (2013) Seawater contribution to polymetallic Ni–Mo–PGE–Au mineralization in Early Cambrian black shales of South China: Evidence from Mo isotope, PGE, trace element, and REE geochemistry. *Ore Geol. Rev.* **52**, 66-84.

Yamashita Y., Takahashi Y., Haba H., Enomoto S. and Shimizu H. (2007) Comparison of reductive accumulation of Re and Os in seawater–sediment systems. *Geochim. Cosmochim. Acta* **71**, 3458-3475.

Yang G., Hannah J. L., Zimmerman A., Stein H. J. and Bekker A. (2009) Re-Os depositional age for Archean carbonaceous slates from the southwestern Superior Province: Challenges and insights. *Earth Planet. Sci. Lett.* **280**, 83-92.

Yudovskaya M. A., Tessalina S., Distler V. V., Chaplygin I. V., Chugaev A. V. and Dikov Y. P. (2008) Behavior of highly-siderophile elements during magma degassing: A case study at the Kudryavy volcano. *Chem. Geol.* **248**, 318-341.

Zektser I. S. and Loaiciga H. A. (1993) Groundwater fluxes in the global hydrologic cycle: past, present and future. *J. Hydrol.* **144**, 405-427.

Zhu B., Becker H., Jiang S., Pi D., Fischer-Gödde M. and Yang J. (2013) Re–Os geochronology of black shales from the Neoproterozoic Doushantuo Formation, Yangtze platform, South China. *Precambrian Res.* **225**, 67-76.

Tables

Table 1. Osmium burial rates in modern marine environments

	Anoxic sediments (Anoxic basins)			Suboxic sediments (Continental margins)				Oxic sediments (Fe-Mn crust & nodules, pelagic carbonates, hemipelagic muds)		
	Black Sea [a]	Cariaco Basin [b]	Saanich Inlet [c]	San Pedro Martir Basin [d]	Carmen Basin [d]	Walvis Bay [d]	Guaymas Basin [e]	Fe-Mn crusts & nodules [f]	Eastern Equatorial Pacific [g]	Japan Sea [h]
Os burial rate ($pg/cm^2/yr$)	2.0−3.1	6.5−9.9	16	12.2	6.9	8.7	2.2−9.5	0.0006	0.03−0.09	0.05-0.11
Range of Os burial rate ($pg/cm^2/yr$)	2−16			2−12				0.0006−0.11		
Modern seafloor area [i] (%)	0.35 [j]			6.00 [k]				93.65		
Os burial flux (kg/yr)	25−202			433−2600				2−372		

[a] Ravizza et al. (1991)

[b] Oxburgh et al. (2007), sediments deposited in the past 15 kyr

[c] Poirier (2006)

[d] Ravizza and Turekian (1992)

[e] Dean (2006)

[f] see calculation steps described in section 2.3.2.

[g] Paquay and Ravizza (2012)

[h] Dalai et al. (2005)

[i] Total seafloor area is 3.61×10^{18} cm^2 (Barnes and Cochran, 1990)

[j] Veeh (1968)

[k] Dunk et al. (2002)

Table 2. Average/median ^{192}Os concentrations (pg/g), $^{192}Os/TOC$ ratios (pg/g/wt.%), and initial $^{187}Os/^{188}Os$ isotope ratios for organic-rich mudrocks distributed into three time bins

Time Interval	n ^{192}Os	Average ^{192}Os (pg/g) [median]	n $^{192}Os/TOC$	Average $^{192}Os/TOC$ (pg/g/wt.%) [median]	n initial $^{187}Os/^{188}Os$ ratio	Average initial $^{187}Os/^{188}Os$ ratio [median]
Ediacaran - Phanerozoic (635 - 0 Ma) all data	33	372 ± 616 [155]	21	97 ± 90 [70]	25	0.64 ± 0.32 [0.60]
Ediacaran - Phanerozoic No transient magmatic-hydrothermal events	27	323 ± 666 [115]	16	76 ± 81 [47]	20	0.74 ± 0.27 [0.69]
Ediacaran - Phanerozoic No South China Ediacaran-Cambrian	31	248 ± 234 [138]	20	90 ± 86 [64]	23	0.61 ± 0.30 [0.59]
Ediacaran - Phanerozoic No anomalously high ^{192}Os concentrations* (635-0 Ma)	25	166 ± 148 [106]	15	66 ± 71 [38]	18	0.71 ± 0.26 [0.65]
Pre-Ediacaran - Proterozoic (2500 Ma - 635 Ma)	13	111 ± 96 [82]	6	32 ± 16 [27]	24	0.46 ± 0.29 [0.43]

Archean (≥2500 Ma)	4	143 ± 143 [100]	1	65 ± n/a [65]	2	0.18 ± 0.04 [0.18]

See Table A.2 and A.3 for data and data sources (n denotes number of samples).

Averages include 1SD.

* Excludes data from late Ediacaran and early Cambrian (555 and 535 Ma) organic-rich mudrocks from South China, and organic-rich mudrocks deposited during transient Mesozoic and Cenozoic magmatic-hydrothermal events. See text for explanation.

Table 3. Summary of the means of 10,000 ^{192}Os bootstrap medians along with 95% confidence intervals for each time bin

Time bin	Mean of 10,000 ^{192}Os bootstrap medians	Bootstrap 95% confidence interval
Ediacaran-Phanerozoic (all data)	187	(91, 329)
Ediacaran-Phanerozoic (no anomalous groups)	112	(72, 168)
Pre-Ediacaran Proterozoic	88	(35, 159)
Archean	157	(25, 347)

Figure Captions

Figure 1. Osmium reservoirs relevant to the modern surficial Os geochemical cycle, accompanied by their present day $^{187}Os/^{188}Os$ isotope ratios and Os concentrations [Os]. HT = high-temperature and LT = low-temperature. References for Os isotopic compositions and concentrations are as follows: cosmic dust (Luck and Allègre, 1983; Walker et al., 2002; Georg et al., 2013); aeolian dust (Peucker-Ehrenbrink and Jahn, 2001; Chen et al., 2016); organic-rich mudrocks (see Table A.1 and reference therein); rivers (a range of estimates is shown for the global average $^{187}Os/^{188}Os$ of rivers, Levasseur et al., 1999; Peucker-Ehrenbrink, 2002; Georg et al., 2013); anoxic muds (Oxburgh et al., 2007; Paquay and Ravizza, 2012); seawater (Sharma et al., 1997; Levasseur et al., 1998; Woodhouse et al., 1999; Chen and Sharma, 2009); groundwater discharge (Paul et al., 2010); oxic sediments (Peucker-Ehrenbrink et al., 1995; Ravizza, 2001; Dalai and Ravizza, 2006); hydrothermal fluids (Peucker-Ehrenbrink and Ravizza, 2000; Sharma et al., 2007b); Fe-Mn crusts (Burton et al., 1999); mantle (Shirey and Walker, 1998).

Figure 2. Examples of possible mass balance solutions to explain the observed (non-anthropogenic) deep seawater $^{187}Os/^{188}Os$ of 1.05. Contributions from different sources

summing to the Os flux (f) in units of kg/yr are shown. HT = high-temperature and LT = low-temperature. (a) Riverine Os flux (275 kg/yr) is the average of the estimated global fluxes of 267 kg/yr from Sharma et al. (2007) and 283 kg/yr from Georg et al. (2013). Groundwater Os flux is from Paul et al. (2010). Osmium fluxes from high- and low-temperature hydrothermal fluids are from Georg et al. (2013). Cosmic Os flux is from Sharma et al. (2007). Aeolian Os flux is from Peucker-Ehrenbrink and Ravizza (2000). For $^{187}Os/^{188}Os$, the lower end of the range of suggested global average $^{187}Os/^{188}Os$ for rivers (1.2−1.5; Levasseur et al., 1999; Peucker-Ehrenbrink, 2002; Georg et al., 2013) and aeolian dust (0.8−1.4; Peucker-Ehrenbrink and Jahn, 2001; Chen et al., 2016) are used. $^{187}Os/^{188}Os$ for hydrothermal fluids and cosmic dust is from Georg et al. (2013). $^{187}Os/^{188}Os$ for groundwater discharge is from Paul et al. (2010). Os fluxes from volcanic aerosols are poorly constrained but are assumed to be 10 kg/yr with a $^{187}Os/^{188}Os$ of 0.2. This Os budget permits a deep-seawater $^{187}Os/^{188}Os$ value of 1.05. Other solutions are possible. For example, diagram (b) shows an example with a higher Os flux (105 kg/yr) from high-temperature hydrothermal fluids than is currently recognized (i.e., there is an extra contribution of Os from ultramafic-hosted hydrothermal systems). In this scenario, the $^{187}Os/^{188}Os$ values of riverine and groundwater can be increased to 1.35 (keeping remaining Os parameters unchanged) to yield the observed deep-seawater $^{187}Os/^{188}Os$ value of 1.05.

Figure 3. Histograms showing Os concentrations (as pg/g ^{192}Os) in organic-rich mudrocks in three different time bins (Archean, pre-Ediacaran Proterozoic, and Ediacaran-Phanerozoic). (A) individual ^{192}Os data points; (B) ^{192}Os time points, where individual ^{192}Os data points are re-assigned to time points rounded to the nearest 5 Ma and average values are calculated for each time point. Counts for >1000 pg/g in (A) and >700 pg/g in (B) represent the total number of data that exceed those values. Sources of data: A - Table A.1; B - Table A.2. References are provided in Table A.3.

Figure 4. Compilation of Os concentration data (as pg/g ^{192}Os) from organic-rich mudrocks through time: a) ^{192}Os concentrations, b) ^{192}Os concentrations normalized to TOC (total organic carbon), c) initial ^{187}Os/^{188}Os isotope ratios (from Re-Os isochron regressions), which reflect the local Os isotope composition of seawater at the time of mudrock deposition. Error bars (2σ) are shown for initial ^{187}Os/^{188}Os isotope ratios. Light blue shaded area represents the range of estimated global average river ^{187}Os/^{188}Os for the present day. Dark blue dashed line represents the present day deep-ocean ^{187}Os/^{188}Os. Purple = Archean (≥2500 Ma), Red = pre-Ediacaran Proterozoic (2500-635 Ma), Green = Ediacaran-Phanerozoic (635-0 Ma). Light grey shaded areas represent the two major oxygenation events: GOE = Great Oxidation Event and NOE = Neoproterozoic Oxidation Event. Dashed lines represent formations with anomalously high ^{192}Os concentrations. PE = Paleocene-Eocene Thermal Maximum event (ca. 56 Ma), CT = Cenomanian-Turonian OAE2 (ca. 93.5 Ma), A = early Aptian OAE1a (ca. 120 Ma), SP = Sinemurian-

Pliensbachian boundary (ca. 190 Ma), TJ = Triassic Jurassic boundary (200-205 Ma), EC = early Cambrian Niutitang Formation (ca. 535 Ma), LE = late Ediacaran Doushantuo Formation (ca. 555 Ma). See Table A.1, A.2, and A.3 for data and data sources.

Figure 5. Extent of correlation between ^{192}Os and TOC contents for all formations in the Os compilation. Formation name and compilation age are shown for each plot. See Table A.1 and A.3 for data and data sources.

Figure 6. Comparison of average ^{192}Os concentrations and average initial $^{187}Os/^{188}Os$ ratios for individual time points in the compilation. "Anomalous group" refers to unusually high ^{192}Os concentrations. PETM = Paleocene-Eocene Thermal Maximum; OAE = ocean anoxic event; T-J boundary = Triassic-Jurassic boundary; S-P boundary = Sinemurian-Pliensbachian boundary; Fm. = Formation. See details in main text and Table A.2 and A.3 for data and data sources.

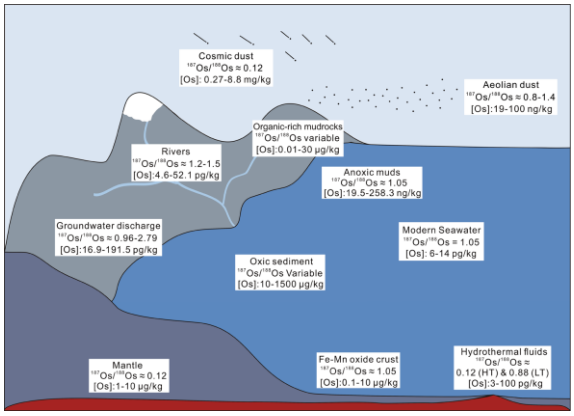

a) an example based on estimated Os fluxes to the ocean

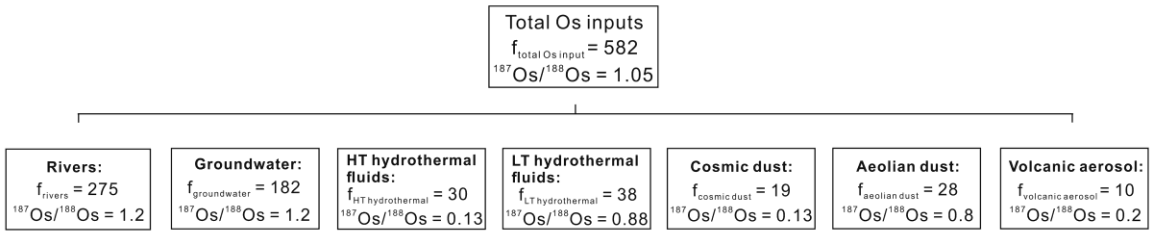

b) an example that takes into account a higher HT hydrothermal Os flux to the ocean